International Journal of Earth Sciences (2021) 110:689–718
https://doi.org/10.1007/s00531-021-01981-6

ORIGINAL PAPER

The Volsci Volcanic Field (central Italy): eruptive history, magma system and implications on continental subduction processes

F. Marra[1] · G. L. Cardello[2] · M. Gaeta[2] · B. R. Jicha[3] · P. Montone[1] · E. M. Niespolo[4,5] · S. Nomade[6] · D. M. Palladino[2] · A. Pereira[6,7,8] · G. De Luca[1] · F. Florindo[1] · A. Frepoli[1] · P. R. Renne[4,5] · G. Sottili[2]

Received: 8 September 2020 / Accepted: 5 January 2021 / Published online: 12 February 2021

Abstract

Here, we report on the Quaternary Volsci Volcanic Field (VVF, central Italy). In light of new $^{40}Ar/^{39}Ar$ geochronological data and compositional characterization of juvenile eruptive products, we refine the history of VVF activity, and outline the implications on the pre-eruptive magma system and the continental subduction processes involved. Different from the nearby volcanic districts of the Roman and Campanian Provinces, the VVF was characterized by small-volume (0.01–0.1 km^3) eruptions from a network of monogenetic centers (mostly tuff rings and scoria cones, with subordinate lava occurrences), clustered along high-angle faults of lithospheric depth. Leucite-bearing, high-K (HKS) magmas (for which we report for the first time the phlogopite phenocryst compositions) mostly fed the early phase of activity (~761–539 ka), then primitive, plagioclase-bearing (KS) magmas appeared during the climactic phase (~424–349 ka), partially overlapping with HKS ones, and then prevailed during the late phase of activity (~300–231 ka). The fast ascent of primitive magma batches is typical of a tectonically controlled volcanic field, where the very low magma flux is a passive byproduct of regional tectonic strain. We suggest that the dominant compressive stress field acting at depth was accompanied by an extensional regime in the upper crust, associated with the gravity spreading of the Apennine chain, allowing the fast ascent of magma from the mantle source with limited stationing in shallow reservoirs.

Keywords Quaternary volcanism · $^{40}Ar/^{39}Ar$ geochronology · Potassic magmatism · Tyrrhenian Sea margin · Central Italy

Introduction

The Volsci Volcanic Field (VVF) (Cardello et al. 2020), previously known (improperly) as Monti Ernici volcanoes (Murchison 1850; Ponzi 1858a, b; Branco 1877), includes the Middle Latin Valley volcanic field (Angelucci et al. 1974; Pasquarè et al. 1985; Narcisi 1986; Frezzotti et al. 2007; Boari et al. 2009; Centamore et al. 2010), and is associated with the potassic magmatism active along the Tyrrhenian coast of central Italy during Quaternary (Fig. 1). Based on isotope geochemical affinity, Peccerillo (2017) grouped the VVF volcanics within the Ernici–Roccamonfina Volcanic Province, distinct from the Roman and Campanian ones.

The Tyrrhenian Sea margin back-arc domain has been affected by extensional tectonics since Pliocene, as a consequence of the retreat of the west-directed Adriatic slab, whereas the central part of the Italian peninsula displays regional uplift that has built the Apennine belt (e.g., Doglioni et al. 1994; Hippolyte et al. 1994; Sartori et al.

✉ F. Marra
fabrizio.marra@ingv.it

1 Istituto Nazionale di Geofisica e Vulcanologia, Rome, Italy

2 Dipartimento di Scienze Della Terra, Sapienza-Università di Roma, Rome, Italy

3 Department of Geoscience, University of Wisconsin-Madison, Madison, USA

4 Department of Earth and Planetary Science, University of California, Berkeley, USA

5 Berkeley Geochronology Center, Berkeley, USA

6 Laboratoire des Sciences du Climat et de l'Environnement (CEA-CNRS-UVSQ), IPSL, Université Paris-Saclay, Gif sur Yvette, France

7 CNRS Laboratoire GEOPS, Université Paris-Saclay, Orsay, France

8 Département Homme et Environnement, UMR 7194, HNHP, Museum National d'Histoire Naturelle, Paris, France

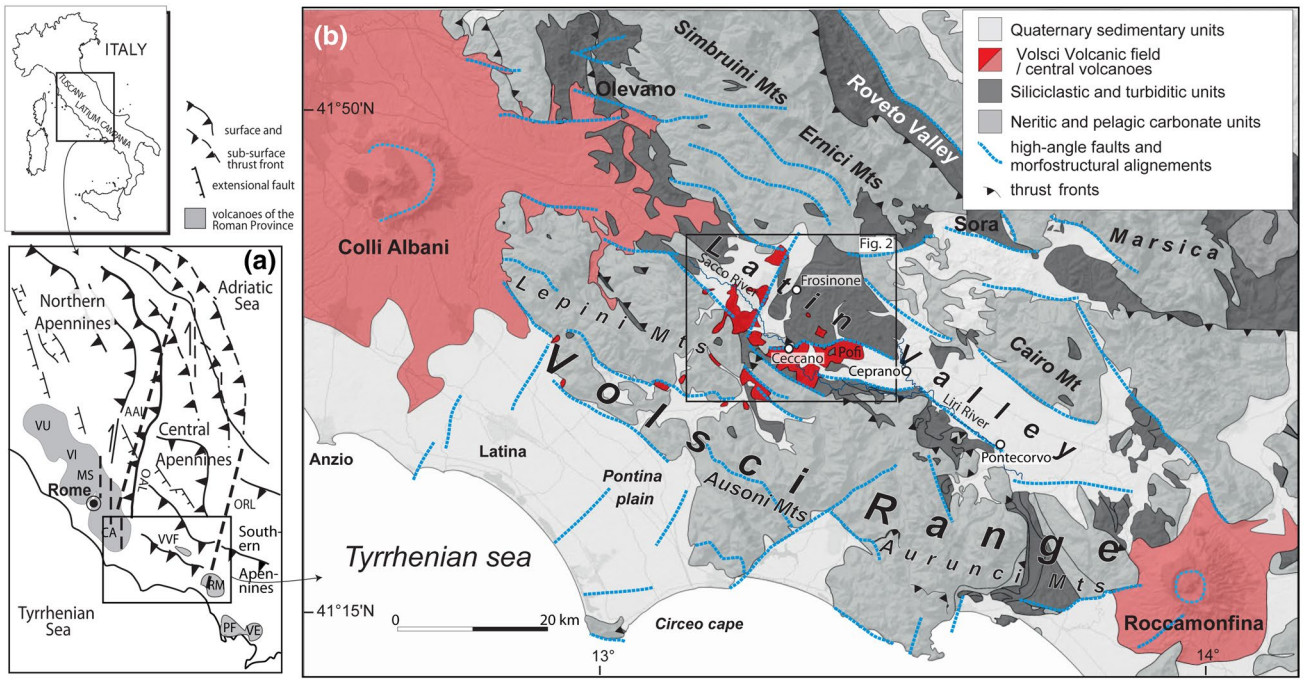

Fig. 1 **a** Structural scheme of Central Italy. Legend: *AAL* Ancona–Anzio Line, *OAL* Olevano–Antrodoco Line, *ORL* Ortona–Roccamonfina Line. Grey areas represent the Quaternary volcanic districts of the "Roman" and "Campanian" Provinces (Peccerillo 2017): *VU* Vulsini, *VI* Vico, *MS* Monti Sabatini, *CA* Colli Albani, *VVF* Volsci Volcanic Field (including the middle Latin Valley or Ernici volcanoes from previous literature); *RM* Roccamonfina, *PF* Campi Flegrei, *VE* Somma–Vesuvius, **b** regional geological sketch map showing the location of the study area

2004; Molli 2008; Carminati et al. 2014; Beaudoin et al. 2017). The development of NW- and NE-striking high-angle normal faults has produced a Horst-and-Graben structure extending from Tuscany to Campania, along which several potassic volcanic districts were active since 0.8 Ma to present (Peccerillo 2017 and references therein).Volcanic activity in the Roman Province, including major caldera-forming explosive events, has occurred since ca. 590–565 ka at the Vulsini, Monti Sabatini and Colli Albani volcanic districts (Fig. 1), and it seems to have ceased progressively from NW to SE since ca. 111 ka (Vulsini), 95 ka (Vico), 70 ka (Sabatini) and 36 ka (Colli Albani) (Barberi et al. 1994; Perini et al. 2004; Palladino et al. 2010; Marra et al. 2016, 2019, 2020a, b). To the south of the VVF, the activity of the Roccamonfina volcano, although poorly constrained geochronologically, seems to have spanned 696 ± 49 to 148 ± 18 ka with potential younger activity (i.e., 53 ± 27 ka, Radicati di Brozolo 1988; Rouchon et al. 2008).

Unlike the other volcanic districts of the Tyrrhenian margin, the VVF eruptive centers occur within the inner Apennine mountain range (Fig. 1). Another peculiarity of the VVF volcanism is the lack of a major volcanic edifice or a central caldera. Instead, the rapid ascent of relatively primitive magmas from the mantle source has produced a network of monogenetic magmatic and phreatomagmatic centers (Boari et al. 2009; Centamore et al. 2010). The reported occurrence of mafic volcanic rock types representative of different magma suites (i.e., ultrapotassic, calc-alkaline and kamafugitic; Boari and Conticelli 2007; Frezzotti et al. 2007; Boari et al. 2009; Centamore et al. 2010; Koornneef et al. 2019) is another intriguing aspect of this volcanic field. These "bullet eruptions", fed by fast ascending magma batches, open a window on mantle source in continental subduction settings.

Prior to this study, the reconstruction of the VVF eruptive history was based on an old set of K–Ar ages spanning 0.7–0.1 Ma (Fornaseri 1985; Basilone and Civetta 1975). However, they lack analytical details and, as for other age determinations performed in the 1970–1980s, their accuracy is questionable (e.g., Karner and Renne 1998). The only recent $^{40}Ar/^{39}Ar$ investigation (Boari et al. 2009) was essentially based on the dating of small-volume lava flows and thus cannot be considered as representative of the whole temporal and compositional spectrum of the VVF activity. We present a new set of $^{40}Ar/^{39}Ar$ dates of VVF eruptive products, integrated with petrographic and microchemical analyses, in the frame of stratigraphic, geomorphologic, structural, and seismological observations. Our work contributes to a comprehensive reconstruction of the VVF eruptive history and feeder magma system, with respect to the

possible geodynamic setting. This provides implications on the broader volcano-tectonic context of the Tyrrhenian Sea margin of central Italy and related hazard assessment.

Geological-structural setting

The study area (Fig. 1) is part of the central Apennines, a mountain chain made up of terrains belonging to different Meso-Cenozoic paleogeographical domains developed after Late Triassic on the southern margin of the rifting Tethys (Parotto and Praturlon 1975; Bernoulli 2001; Cardello and Doglioni 2015). The study area is located between the Simbruini–Ernici–Cairo mountain ridges and the Volsci Range (Fig. 1), which belong to the Latium–Abruzzi neritic carbonate domain (upper Triassic-middle Miocene), covered by middle Miocene to early Pliocene syn-orogenic siliciclastic deposits (Centamore et al. 2007 and references therein). Overall, the central Apennine fold-and-thrust belt is characterized by tectonic structures showing northeast polarities due to Late Tortonian–Early Messinian compressional tectonics. The Simbruini and Ernici Mts. are built up of several NW–SE striking imbricate thrust sheets that overthrust onto Tortonian-lower Messinian terrigenous deposits within the Latin and Roveto valleys (Fig. 1; Devoto 1967; Parotto 1971; Fabbi and Santantonio 2018). The Volsci Range is organized in several thrust sheets defined by fore- and back-thrusts, cross-cut by a system of conjugated synthetic and antithetic Quaternary normal faults (Cavinato et al. 1994; Cosentino et al. 2002; Sani et al. 2004; Parotto and Tallini 2013). The Latin Valley is a graben comprised between two ~ N–S trending major tectonic lines with polyphase activity, namely the Ortona–Roccamonfina (or Volturno–Sangro Line; Locardi 1982) and the Olevano–Antrodoco–Sibillini lines (e.g. Pizzi and Galadini 2009). The latter can be considered as the positive re-activation of pre-existing continental break-up structures. The Ancona–Anzio line (Castellarin et al. 1978) results from a transpressive thrust system (Cipollari and Cosentino 1991; Koopman 1983; Lavecchia 1985; Butler et al. 2006, and references therein).

Locally, besides the dominant NW- and the minor NE-trending structures, the study area has also been affected by N- to NNE- and E- to ENE-striking high-angle faults with strike-slip kinematics up to Middle Pleistocene (Sani et al. 2004; Centamore et al. 2010; Cardello et al. 2020). The strike-slip tectonics have been previously associated with the volcanic centers of the VVF, whose compositions show a mantle origin, thus suggesting a lithospheric depth for these structures (Acocella et al. 1996).

In the mountain areas adjoining the Latin Valley, the compressional structures are cross-cut by a nearly coaxial system of mainly Late Pliocene–Quaternary high-angle extensional faults (Cardello et al. 2020). These faults likely controlled the formation and growth of intramountain basins. An example of extensional tectonics is represented by two main morpho-structural elements within the Latin Valley (Fig. 1): the Liri Valley to the SE, and the Sacco Valley to the NW corresponding to the middle sector of the NW-trending graben also known as "Middle Latin Valley".

The most recent tectonic phase along the axial zone of the Apennines (i.e., Marsica; Fig. 1) is expressed by a set of mainly NW-trending normal or normal oblique fault systems (Calamita and Pizzi 1994; Lavecchia et al. 1994; Ghisetti and Vezzani 1999; Piccardi et al. 1999; Morewood and Roberts 2000; Blumetti and Guerrieri 2007; Pizzi and Galadini 2009). The present-day stress field is characterized by a prevalent, ~ NE–SW oriented, extension, derived by stress indicators (Montone and Mariucci 2019). The chronological range of the extensional tectonics is poorly constrained, although it is generally assigned to the Quaternary (e.g., Sani et al. 2004). However, an intensive extensional phase related to the formation of the Liri lacustrine basin (Lirino Lake Synthem) occurred during the Middle Pleistocene (Centamore et al. 2010).

Seismic features

Here, we present a brief summary of the seismicity affecting the Latin Valley and surrounding area in the period 2009–2013 (Frepoli et al. 2017), implemented by new data recorded over the period 2014–2019, aimed at providing a picture of the present stress field, compared with the Middle Pleistocene tectonic regime. Figure 2 displays the seismicity (M_L 0.4–4.7) recorded by the permanent (Seismic National Network, RSN) and temporary stations of the Istituto Nazionale di Geofisica e Vulcanologia (INGV), and the regional networks of Abruzzo (RSA; De Luca 2011) and Molise (see Frepoli et al. 2017 for the employed methodology). All the waveforms of this seismicity were re-picked to obtain both more accurate arrival times of *P*- and *S*-waves and a larger number of first-motion polarities with respect to the routine procedure for the compilation of INGV seismic bulletins. Four NE-striking cross-sections in Fig. 2 show the distribution of seismicity at depth.

Seismicity concentrates within the axial part of the Apennines. Here, the most relevant seismic sequence occurred on February 16th, 2013, in the Pescasseroli–Sora area, with a magnitude M_L 4.7 mainshock and with ~ 350 aftershocks. The hypocenter depth of this sequence extended down to 18 km, with a pronounced maximum between 8 and 15 km. The most recent seismicity (period 2014–2019) overlaps the previous one (period 2009–2013) in the same areas. In contrast, seismicity fades out along the Volsci Range, although present in the Pontina Plain (W of the Volsci Range area). Seismic events are scattered within the Latin Valley and, in particular, are rare in the VVF area. Here, seismicity affects

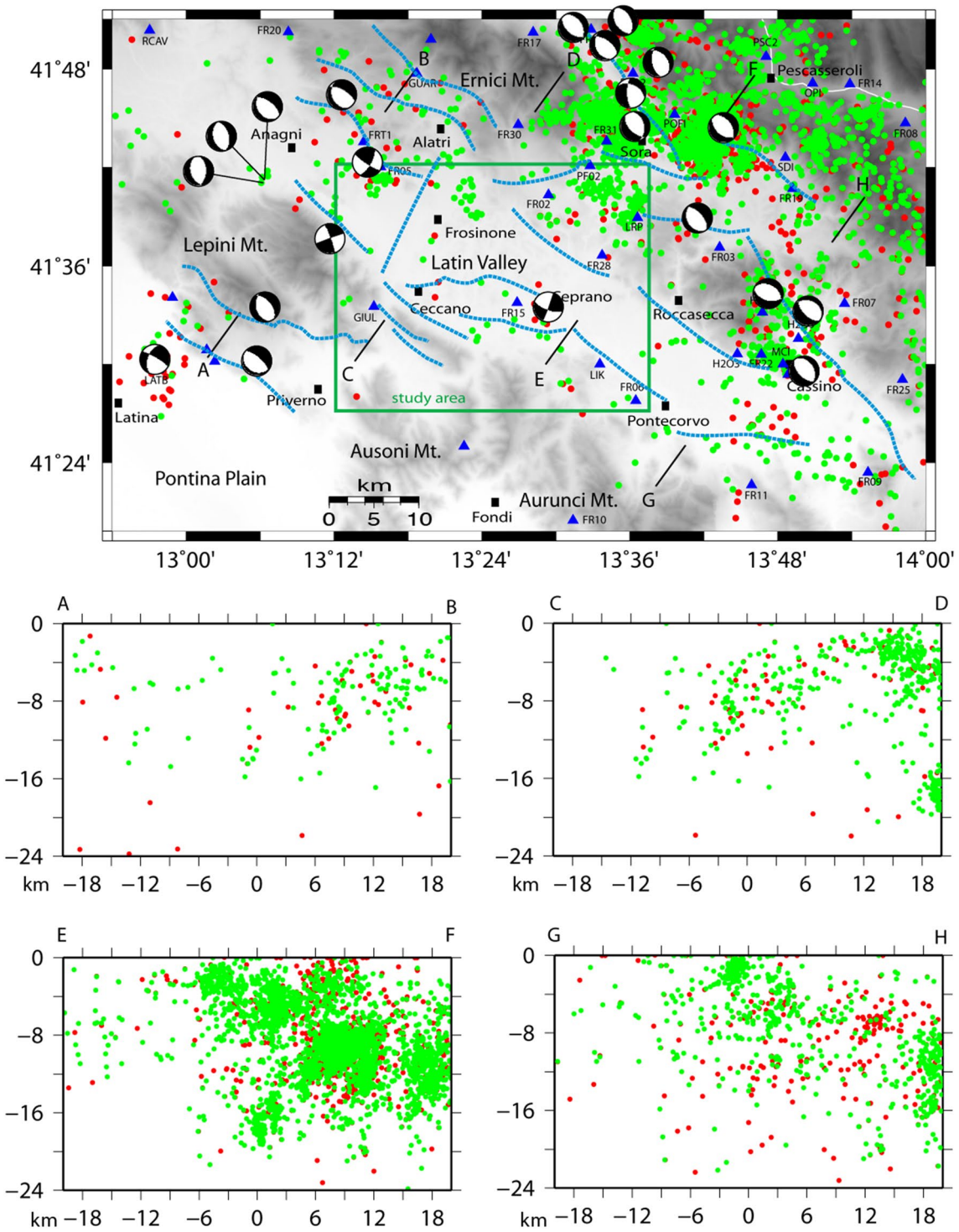

Fig. 2 Map of the seismicity (M_L 0.4–4.7) recorded in the period 2009–2013 (red dots) and 2014–2019 (green dots) by permanent and temporary stations of INGV and the regional networks of Abruzzo and Molise in the study area and in the surrounding region. Inferred faults (dashed blue lines) are also reported. Four NE–SW cross-sections show the seismicity distribution at depth

the upper portion of the crust and is linked to the widespread NE–SW oriented extensional regime, as shown by the normal faulting focal mechanism of the most constrained solutions of the dataset (Fig. 2).

The Volsci Volcanic Field (VVF)

Based on the overall areal distribution of the monogenetic centers, extending (from east to west) from the Sacco River Valley, through the Volsci Range, as far as the Pontina Plain (Fig. 2), and following Cardello et al. (2020), here we define the previously known Monti Ernici or Middle Latin Valley volcanoes as the Volsci Volcanic Field (VVF), consistent with the geographic and historical pertinence of ancient Italic populations. The VVF extends in two main geomorphic settings (Fig. 3): (1) the Sacco River Valley (or Middle Latin Valley) to the E, and (2) the mountain backbone and foothill of the Volsci Range (as far as the adjoining Pontina Plain) to the W, broadly corresponding to the Frosinone foredeep and the Volsci Range carbonate belt structural domains, respectively.

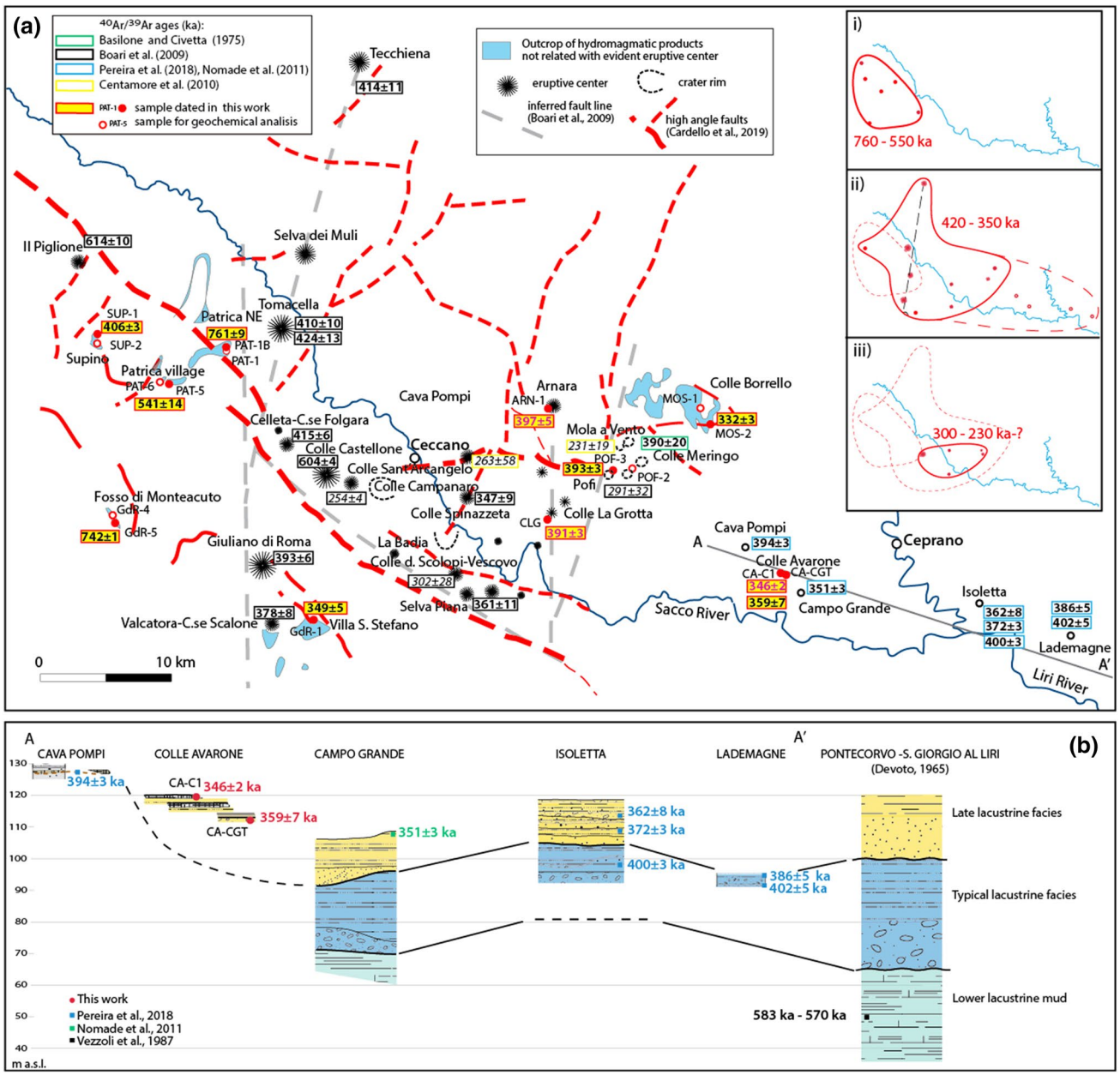

Fig. 3 **a** Sketch map showing the locations and preferential alignments of VVF eruptive centers (simplified after the Geologic Map of Italy; Accordi et al. 1966; Alberti et al. 1975; Centamore et al. 2010). Radioisotopic ages from literature (in italics those with poor analytical constraints) and the present study are reported. Areal vs. temporal migration of the volcanic activity is shown in insets i–iii. **b** Cross-correlation chart showing the geochronological constraints to the sedimentary fill of the Liri Basin based on distal volcanic deposits intercalated in the fluvial-lacustrine successions

The VVF terrains are mostly pyroclastic fall and surge deposits from low-intensity and low-magnitude explosive (i.e., Hawaiian–Strombolian and phreatomagmatic) eruptive events, and subordinate lava flows and plateaus from effusive activity (Centamore et al. 2010; Cardello et al. 2020 and reference therein). More specifically, based on well-established field criteria, loose to welded, well-sorted, clast-supported beds of moderately vesicular, scoria, and spatter lapilli and blocks are interpreted as the products of fallout from Hawaiian–Strombolian fountains. Stratified deposits of fine to coarse ash and lapilli, characterized by poorly vesicular juvenile scoria, abundant lithics of the sedimentary substrate, with possible occurrence of accretionary lapilli and a variety of bedforms (e.g., planar- and cross-lamination, low-angle dunes), are attributed to phreatomagmatic base surges.

Overall, the geologic structural setting likely controlled the location of volcanic activity and the erupted magma compositions, as well as the style of eruptive events. It appears that deep-seated high-angle faults primarily controlled magma ascent from the source, while the extensional faults of the Meso-Cenozoic carbonate substrate determined the distribution pattern of eruptive centers, and favored the repeated, relatively fast ascent of primitive, small magma batches, feeding small-scale events (Centamore et al. 2010; Cardello et al. 2020). In particular, the southern part of the Sacco River Valley (south of Ceccano) is a continental basin developed in an asymmetric graben-like structure bounded by the ENE-striking Ceccano Fault to the north and a NW-striking normal fault system to the south, bounding the Volsci Range and the Middle Latin Valley Graben, onto which several eruptive centers are seated (Fig. 3). Another alignment of eruptive centers (including the Tecchiena, Selva dei Muli, Celleta and Giuliano di Roma centers; Fig. 3) occurs along a NNE-striking lineament. identified as a right-lateral fault by Acocella et al. (1996) and Sani et al. (2004).

In addition, the wall rock architecture, characterized by rock types with highly different degrees of permeability (i.e., platform carbonates vs. pelitic-arenaceous, volcanic layers), and the local presence of closed/suspended aquifers, favored the explosive interaction of mafic magmas with groundwater. The different types and proportions of lithic inclusions in the phreatomagmatic deposits provide indications on the depths of magma-wall rock interaction, which took place at multiple levels ranging from relatively shallow Miocene siliciclastic terrains (e.g., Frosinone formation; Centamore et al. 2010) to deeper Meso-Cenozoic carbonates (Cardello et al. 2020). Besides the predominant magmatic or phreatomagmatic character of specific eruptive centers, typically, individual eruptions from VVF monogenetic centers were often characterized by transitions from mildly explosive, magmatic phases (i.e., Hawaiian–Strombolian, with possible associated effusive activity) to phreatomagmatic phases with higher degrees of magma fragmentation and explosivity. The low viscosities of VVF mafic magmas and the decreasing magma discharge rates in the late stages of individual eruptions favored explosive magma–water interaction.

Overall, volcanic terrains (including their reworked equivalents) are scattered over an area of nearly 600 km^2, covering ~ 100 km^2. Relic morphologies (partially preserved crater rims and volcanic edifices) and lithofacies associations of erupted products indicate a network of rooted monogenetic centers, including scoria and spatter cones, maar-tuff rings and tuff cones. The VVF was thus characterized by areal volcanic activity through time, with the partial exception of the Pofi composite volcanic edifice, resulting from clustered eruptive centers.

An integrated Unconformity-Bounded Stratigraphic Unit (UBSU) and lithostratigraphic setting for the eastern part of the VVF is provided by the 1:50,000 Geologic Map of Italy, Sheet 402-Ceccano (CARG Project; Centamore et al. 2010), based on the fragmentary stratigraphic relationships reconstructed in the field, rock type compositions and a few new geochronological data. Up to now, available geochronological data did not allow for defining the onset and timing of the VVF eruptive activity. Based on previous geochronological data (see the following section), volcanic activity developed in the time span of ca. 700–100 ka, and thus was roughly contemporaneous with that of the nearby potassic volcanic districts of the Roman Province (Colli Albani and Sabatini; Gaeta et al. 2016; Marra et al. 2014, 2016, 2019, 2020a, b; Sottili et al. 2010).

Compositionally, the VVF-erupted magmas are poorly to slightly differentiated. According to available data, mostly referring to lava rock types, they range from K-basalts to K-foidites in the TAS diagram (Boari et al. 2009). A wider compositional dataset, also including a variety of pyroclastic products, is reported in Centamore et al. (2010) for the eastern VVF centers (Ceccano and Pofi areas).

Previous studies (Basilone and Civetta 1975; Civetta et al. 1979, 1981; Frezzotti et al. 2007; Boari et al. 2009) recognized four main types of parental magmas and related evolutionary series: (1) ultrapotassic-kamafugitic (KAM), (2) high-potassic (HKS); (3) shoshonitic (SHO) and (4) sub-alkaline (CA). To favor the comparison with the new geochronological data, obtained exclusively from pyroclastic products, in the following, we group the literature data in HKS and KS (potassic) rock types, including KAM plus HKS and SHO plus CA, respectively. The rationale of our choice is in the small size of the analyzed juvenile scoria clasts that generally can be compared with the lava flow compositions exclusively on the basis of textural and microchemical features determined in thin section. The HKS group comprises leucite-bearing lava flows, different from the KS lavas, which contain plagioclase and commonly lack leucite. Compatible with the usually low

porphyricity degrees (and variably altered groundmass) of juvenile scoria clasts, the HKS vs. KS distinction is also applied to pyroclastic products, based on the leucite vs. plagioclase occurrence (both from literature data and new petrographic observations).

Geochronology of the VVF

The published ages for the VVF eruptive products are summarized in Table 1. Available whole rock K/Ar ages should be considered with caution, because of their large uncertainties and the possible bias towards older ages due to contamination from xenocrysts with inherited ^{40}Ar. To compare the geochronologic dataset discussed later in this paper, we re-calculated the ^{40}Ar/^{39}Ar ages reported in Boari et al. (2009) (mostly obtained from lava groundmass) according to the standard age used for our data (i.e., 28.201 ± 0.046 Ma for FCT sanidine, Kuiper et al. 2008; equivalent to ACs at 1.1848 ± 0.0012 Ma, Niespolo et al. 2017). For further discussion of accuracy and reliability of literature ages, see "New geochronologic constraints".

So far, the oldest reported ages are from the Piglione (614 ± 10 ka, Boari et al. 2009; Table 1) and Colle Castellone (604 ± 4 ka, Boari et al. 2009) eruptive centers. In addition, two tephra layers in the lacustrine deposits of the Pontecorvo area (LRN1 subsynthem; Centamore et al. 2010), K–Ar dated to 583 ± 11 and 570 ± 11 ka, constrain the oldest eruptive events in the eastern VVF (cf. Sheet 402-Ceccano; Centamore et al. 2010). The peak of VVF activity occurred between 430 and 350 ka, as shown by a cluster of effusive and mildly explosive eruptions in the Pofi area (e.g., Fosso Meringo phonotephritic lavas, 390 ± 20 ka to 400 ± 10 ka, Basilone and Civetta 1975) and SE of Ceccano (e.g., Colle Selva Piana basaltic lavas, 361 ± 11 ka; Colle Spinazzeta basaltic lava dyke, 347 ± 7 ka, Boari et al. 2009) that were broadly contemporaneous with the Celleta (415 ± 6 ka), Tecchiena (414 ± 11 ka) and Giuliano di Roma (393 ± 6 ka) lava flows and the Valcatora lava dyke (378 ± 8 ka; Boari et al. 2009). In addition, the following volcanic activity was broadly contemporaneous in the Pofi and Ceccano areas: e.g. the age of 291 ± 32 ka reported by Boari et al. (2009) for the phonotephrite scoria products of the Pofi volcano; the Colle Capirolo trachybasaltic lava (263 ± 58 ka, Centamore et al. 2010) and the Colle Sant'Arcangelo lava (254 ± 4 ka; Boari et al. 2009). Up to now, the youngest ages pertain to the Mola a Vento unit of the Pofi area (190 ka, Fornaseri 1985; 231 ± 19 ka; Centamore et al. 2010). However, the results of our study and the re-examination of previous analytical data suggest that the age of the youngest activity phase needs to be re-considered.

Methods

Sampling

To provide ^{40}Ar/^{39}Ar age constraints to the widespread VVF phreatomagmatic activity, we sampled the products of rooted eruptive centers in the Volsci Range backbone. Of these, only five samples (PAT-1B, PAT-5, SUP-1, GdR-1, GdR-5; Fig. 3) contained datable K-bearing mineral phases and were processed. Moreover, we dated four samples from the eruptive centers of the central sector of the Middle Latin Valley (ARN-1, POF-3, CLG, MOS-2; Fig. 3). In addition, we dated a pair of volcaniclastic horizons (CA-C1, CA-CGT) interbedded in the uppermost portion of the Liri Basin lacustrine deposits (Colle Avarone locality, nearby Ceprano; Fig. 3), to put constraints to the final stages of sedimentation within the Liri Basin, hosting the remains of a calvarium belonging to the "*Homo heidelbergensis*" species (i.e., namely *Homo cepranensis*, Ascenzi et al. 2000; Nomade et al. 2011, Manzi 2016).

Petrographic and microchemical analyses

Textural aspects of the recovered samples were first analyzed in thin section at the optical microscope and successively at the Scanning Electron Microscopy (SEM), using a FEI Quanta-400 at the Earth Sciences Department (Sapienza University, Rome, Italy). Phase compositions were analyzed at the Consiglio Nazionale delle Ricerche-Istituto di Geologia Ambientale e Geoingegneria (CNR-IGAG, Rome), by a Cameca SX50 electron microprobe equipped with five wavelength dispersive spectrometers (WDS). Quantitative compositional analyses were performed using 15 kV accelerating voltage, 15 nA beam current and beam diameter of 1 µm. As standards, we employed metals for Mn and Cr, jadeite for Na, wollastonite for Si and Ca, orthoclase for K, corundum for Al, magnetite for Fe, rutile for Ti and periclase for Mg. Counting times were 20 s for elements and 10 s for backgrounds. Light elements were counted first to prevent loss by volatilization. The PAP correction method (Pouchou and Pichoir 1991) was used. The essential features of the sampled products are reported in Tables 2 and 3; further details on sampled outcrops are provided in Supplementary File #1.

^{40}Ar/^{39}Ar analyses

Samples for ^{40}Ar/^{39}Ar analyses were prepared at the Laboratoire des Sciences du Climat et de l'Environnement facility (CNRS-CEA, Gif-sur-Yvette), France. After having been

Table 1 Summary of literature K/Ar and $^{40}Ar/^{39}Ar$ ages for VVF eruption products (for the HKS vs. KS characterization see "The Volsci Volcanic Field (VVF)")

Author	Method	Dated phase	Rock type	Sample label	Locality	Latitude	Longitude	Plateau age (ka) × total age	2σ
(1)	*K/Ar*	*Whole rock*	*HKS-lava*	*S 18*	*Pozzo Colonnello (Pofi)*	–	–	*80*	±*40*
(1)	*K/Ar*	*Whole rock*	*HKS-lava*	*S 22*	*Colle Vitelli (Pofi)*	*41° 34′ 15.55″ N*	*13° 24′ 47.07″ E*	*110*	±*30*
(1)	*K/Ar*	*Whole rock*	*HKS-lava*	*S 18*	*Pozzo Colonnello (Pofi)*	-	-	*120*	±*60*
(1)	*K/Ar*	*Whole rock*	*HKS-lava*	*S 22*	*Colle Vitelli (Pofi)*	*41° 34′ 15.55″ N*	*13° 24′ 47.07″ E*	*130*	±*30*
(1)	*K/Ar*	*Whole rock*	*KS-lava*	*S 4*	*Colle del Vescovo*	*41° 31′ 44.26″ N*	*13° 21′ 25.10″ E*	*170*	±*80*
(1)	*K/Ar*	*Whole rock*	*KS-lava dyke*	*S 9*	*Colle Spinazzeta*	*41° 33′ 13.46″ N*	*13° 20′ 59.73″ E*	*180*	±*90*
(1)	*K/Ar*	*Whole rock*	*KS-lava*	*ERN 3*	*Colle Spinazzeta*	*41° 33′ 13.46″ N*	*13° 20′ 59.73″ E*	*200*	±*40*
(1)	*K/Ar*	*Whole rock*	*HKS-lava*	*M 2*	*Colle Celleta*	*41° 34′ 58.85″ N*	*13° 17′ 34.62″ E*	*220*	±*20*
(1)	*K/Ar*	*Whole rock*	*KS-lava dyke*	*S 9*	*Colle Spinazzeta*	*41° 33′ 13.46″ N*	*13° 20′ 59.73″ E*	*230*	±*110*
(2)	Ar/Ar	K-poor feldspar	HKS-scoria	FT0 28	Mola a Vento	-	-	231	±19
(1)	*K/Ar*	*Whole rock*	*HKS-lava*	*S1*	*Colle Spinazzeta*	*41° 33′ 13.46″ N*	*13° 20′ 59.73″ E*	*240*	±*100*
(1)	*K/Ar*	*Whole rock*	*HKS-lava*	*M 2*	*Colle Celleta*	*41° 34′ 58.85″ N*	*13° 17′ 34.62″ E*	*250*	±*20*
(3)	Ar/Ar	Leucite	HKS-lava	ERN86	Colle Sant' Arcangelo	41° 33′ 42″ N	13° 18′ 29″ E	252	±4
(2)	Ar/Ar	Groundmass	KS-lava	TV002	Colle Capirolo	–	–	263	±58
(3)	Ar/Ar	Groundmass	KS-scoria	ERN100	Pofi, village	41° 33′ 50″ N	13° 24′ 50″ E	289	±32
(1)	*K/Ar*	*Whole rock*	*HKS-lava*	*M 5*	*Colle Cerroni*	*41° 34′ 10.36″ N*	*13° 17′ 0.55″ E*	*290*	±*20*
(3)	Ar/Ar	Groundmass	KS-lava	ERN94	Colle del Vescovo	41° 32′ 09″ N	13° 21′ 20″ E	300	±28
(3)	Ar/Ar	Groundmass	KS-neck	ERN20	Colle Spinazzeta	41° 33′ 13″ N	13° 21′ 00″ E	345	±7
(2)	Ar/Ar	Groundmass	KS-lava	TV001	Selva Piana	–	–	350	±100
(3)	Ar/Ar	Groundmass	KS-lava	ERN91	Selva Piana	41° 31′ 35″ N	13° 21′ 21″ E	359	±11
(1)	*K/Ar*	*Whole rock*	*KS-lava*	*ERN 7*	*Colle del Vescovo*	*41° 31′ 44.26″ N*	*13° 21′ 25.10″ E*	*370*	±*40*
(4)	*K/Ar*	*Whole rock*	*HKS-lava*	*Er-5*	*Pofi, highway*	*41° 33′ 28.62″ N*	*13° 24′ 51.98″ E*	*370*	±*20*
(3)	Ar/Ar	Groundmass	HKS-lava dyke	ERN23	Valcatora	41° 31′ 2.24″ N	13° 17′ 12.07″ E	376	±8
(4)	K/Ar	Leucite	HKS-lava	Er-3	Fosso Meringo (Pofi)	41° 34′ 44.44″ N	13° 25′ 37.35″ E	390	±20
(3)	Ar/Ar	Groundmass	HKS-lava	ERN50	Giuliano di Roma	41° 21′ 03″ N	13° 16′ 42″ E	391	±6
(4)	K/Ar	Leucite	HKS-lava	Er-1	Giuliano di Roma	41° 32′ 9.83″ N	13° 16′ 43.30″ E	400	±20
(1)	*K/Ar*	*Biotite*	*HKS-pyroclastic rock*	*S10*	*Patrica*	*41° 35′ 26.71″ N*	*13° 14′ 30.03″ E*	*400*	±*80*
(4)	K/Ar	Leucite	HKS-lava	Er-5	Pofi, motorway	41° 33′ 28.62″ N	13° 24′ 51.98″ E	400	±10

Table 1 (continued)

Author	Method	Dated phase	Rock type	Sample label	Locality	Latitude	Longitude	Plateau age (ka) × total age	2σ
(3)	Ar/Ar	Phlogopite	HKS-pyroclastic rock	ERN101	La Tomacella, upper	41° 36′ 27.70″ N	13° 17′ 3.98″ E	407	± 10
(3)	Ar/Ar	Groundmass	HKS-lava	ERN34	Tecchiena	41° 41′ 09″ N	13° 19′ 20″ E	412*	± 11
(3)	Ar/Ar	Groundmass	HKS-lava	ERN60	Celleta	41° 34′ 17″ N	13° 17′ 34″ E	413	± 6
(4)	*K/Ar*	*Whole rock*	*HKS-lava*	*Er-1*	*Giuliano di Roma*	*41° 32′ 9.83″ N*	*13° 16′ 43.30″ E*	*420*	*± 40*
(3)	Ar/Ar	Phlogopite	HKS-pyroclastic rock	ERN102	La Tomacella, lower	41° 36′ 30.65″ N	13° 17′ 0.64″ E	421	± 13
(1)	*K/Ar*	*Whole rock*	*HKS-lava*	*S 14*	*Pofi*	*41° 33′ 52.28″ N*	*13° 24′ 50.75″ E*	*430*	*± 20*
(4)	K/Ar	Leucite	HKS-lava	Er-4	Contrada Roana	41° 39′ 49.79″ N	13° 18′ 8.76″	540	± 20
(3)	Ar/Ar	Leucite	HKS-lava	ERN56	Colle Castellone	41° 34′ 02″ N	13° 18′ 07″ E	600	± 4
(3)	Ar/Ar	Groundmass	HKS-lava	ERN40	Piglione	41° 37′ 34″ N	13° 12′ 38″ E	610	± 10
(4)	*K/Ar*	*Whole rock*	*HKS-lava*	*Er-2*	*Colle Castellone*	*41° 33′ 56.20″ N*	*13° 18′ 9.18″ E*	*680*	*± 20*
(4)	*K/Ar*	*Leucite*	*HK-lava*	*Er-2*	*Colle Castellone*	*41° 33′ 56.20″ N*	*13° 18′ 9.18″ E*	*700*	*± 20*

Age values with uncertain accuracy and reliability of analytical procedures (see text) are reported in Italics

References: (1) Cortesi in Fornaseri (1985); (2) Centamore et al. (2010); (3) Boari et al. (2009); (4) Basilone and Civetta (1975)

crushed, sieved and cleaned in distilled water in an ultrasonic bath, the clean portions coarser than 840 µm (> 20 mesh) and 840–600-µm sized (30–20 mesh) were selected to extract K-bearing crystals suitable for dating (feldspars and/or leucite). For each sample, at least 50 unaltered crystals were carefully handpicked under a binocular microscope after magnetic separation. To eliminate potential adhering groundmass residues on the selected crystals, the latter were finally leached with a 5–7% HF acid solution and cleaned several times using distilled water in an ultrasonic bath.

Two distinct irradiations and analyses have been performed, as follows. Samples CA-C1, CA-CGT, MOS-2, ARN-1 and CLG were irradiated in the Cd-lined, in-core CLICIT facility of the Oregon State University TRIGA reactor and analyzed at the Berkeley Geochronology Center facility (BGC; California, USA), using a MAP 215-C mass spectrometer (MAP 1), following procedures described in Giaccio et al. (2019). Samples GDR-1, GDR-5, SUP-1, POF-3, PAT-1B and PAT-5 were analyzed at the WiscAr Laboratory of University of Wisconsin–Madison (USA), using a Noblesse 5-collector mass spectrometer, following procedures described in Jicha et al. (2016). All ages are calculated according to the fluence monitor age of Alder Creek sanidine (ACs = 1.1848 ± 0.0012 Ma (Niespolo et al. 2017) and all ages are reported to the precision level of 2σ standard deviation. Detailed procedures and full methods for $^{40}Ar/^{39}Ar$ data acquisition are reported in Supplementary File #2.

Results

Field aspects of the sampled volcanics

We conducted a new geomorphological study, based on combined analyses of satellite images and 1:25,000 topographic maps, which allowed us to outline the relationships among the identified morpho-structural lineaments and the locations of the VVF rooted eruptive centers (Fig. 3). The latter include monogenetic eruptive centers of magmatic (Strombolian scoria cones with associated lava flows) and phreatomagmatic (tuff ring relics) origin, located both in the Volsci Range carbonate mountain backbone setting (i.e., the Fosso di Monteacuto, Villa S. Stefano, Patrica, and Supino phreatomagmatic occurrences) and in the Middle Latin Valley graben (i.e., the Arnara scoria cone and the Pofi composite edifice, resulting from coalescent scoria cones and tuff rings, with associated lava flows). We notice that these eruptive centers, within the general VVF volcano-tectonic framework, are preferentially located along major morphologic breaks, which are associated with the occurrence of major faults cross-cutting all the units of the rock substrate.

Typically, phreatomagmatic deposits share the following lithofacies association.

Along with planar to cross-bedded, occasionally accretionary lapilli-bearing, ash deposits from base surges, alternating with thin, scoria lapilli fallout layers (Fig. 4a, b, e), a peculiar lithology is represented by the peperino-type pyroclastic current deposits (Fig. 4c). The latter mostly occurs in the eruptive centers of the Volsci Range mountain setting (e.g., Fosso di Monteacuto, Patrica, Patrica NE, Villa S. Stefano). This term derives from the Italian word "pepe" for pepper and applied to phreatomagmatic deposits characterized by massive to faintly stratified texture, strongly lithified grey ash matrix, containing white and black, lithic lapilli and blocks (i.e., respectively, carbonate and lava or holocrystalline mafic inclusions), as well as leucite (often turned to analcime), clinopyroxene and dark mica crystals, and occasional accretionary lapilli. This lithofacies reaches up to a few tens of meters in thickness where channeled in response to paleotopography (e.g., at the bottom of stream incisions near Patrica village). In addition, strongly lithified, granular massive beds made up of well-sorted, fine scoria lapilli, with pervasive interstitial calcite are found intercalated within laminated surge beds (Fig. 4d).

Ashy base surge deposits with intervening, poorly consolidated scoria lapilli fallout beds from Strombolian activity are also found (Fig. 4f), and they display variable degrees of preservation or reworking (e.g., Fosso di Monteacuto, Supino, Villa S. Stefano).

Due to the uncertain identification of the juvenile fraction in the peperino facies, $^{40}Ar/^{39}Ar$ analyses were performed on 20–50 loose crystals from the matrix of the associated base surge and/or scoria fall deposits (i.e., samples SUP-1, PAT-5, PAT-1B, GdR-1, and GdR-5).

Of note, different from the Volsci Range setting, phreatomagmatic surge deposits in the Pofi–Arnara area lack the typical peperino lithofacies, and they are rich in sandstone and pelite clasts from the Miocene siliciclastic substrate (i.e., Frosinone formation; Centamore et al. 2010).

Clear evidence of relic morphologies (e.g., maar crater rims) or proximal (near-vent) facies (evidenced by occurrence of ballistic clasts with impact sags and of supercritical dune bedforms) are scarcely preserved in the phreatomagmatic examples of the Volsci Range mountain setting. However, a number of observations favor a near-vent location, such as the occurrence of coarse lithic lapilli and blocks (even a few decimeters in size) with variable degrees of thermometamorphism, as well as of lithic-rich breccia horizons or lenses in the peperino deposits, up to several meters in thickness.

On the other hand, associated magmatic and phreatomagmatic deposits in the Middle Latin Valley (i.e., Pofi, Colle La Grotta, Arnara; Table 2) show unambiguous evidence of a local origin from rooted eruptive centers, which partially preserved their morphologies.

Pofi, the most prominent volcanic center in the study area, is a polygenetic edifice, characterized by prevailing Strombolian (lapilli and scoria fallout deposits) and associated effusive (including the major Fosso Meringo lava flow; Centamore et al. 2010) activities, and subordinate phreatomagmatic activity. Among the cluster of eruptive centers at Pofi, here we considered the Strombolian scoria fall products of the main scoria cone (sample POF-3) (unit POF_a; Centamore et al. 2010). The local occurrences of welded spatter deposits, small lava tongues and a lava dyke, consistently indicate rooted volcanic activity.

In addition, we dated the phreatomagmatic products of Colle La Grotta (sample CLG), attributed to the early eruptive phase of the Pofi volcano (unit ULG; Centamore et al. 2010), which in some places are associated with Strombolian fallout deposits containing black scoria lapilli, bombs, and sandstone blocks with impact sags. Sample ARN-1 was collected from the products of Arnara, which is a partially preserved scoria cone from Strombolian activity (Fig. 3) with subordinate phreatomagmatic phases. Juvenile scoria lapilli and bombs are phonotephritic in composition (Centamore et al. 2010).

Finally, we dated an ash deposit at Colle Borello locality (NE of Pofi; Fig. 3) from the basal part of the local succession, also including coarse ash and scoria lapilli fallout layers and reworked deposits, which are mapped as the stratigraphically highest volcanic unit (unit UBO; Centamore et al. 2010).

Sample localities are reported in Fig. 3 and in Supplementary File #1. In the next section, we describe the relevant mineralogical-petrographic and geochemical features of the sampled material (Table 2). In the next following section, we report the main features of the deposits that were dated by $^{40}Ar/^{39}Ar$ method (Table 3).

Texture and microchemistry of scoria clasts

Scoria clasts in the study products show sub-aphyric, hypocrystalline and scarcely vesicular textures, with phenocryst (> 500 μm) proportions less than 10 vol.%, whereas microphenocrysts (500–100 μm) are, generally, abundant (Table 2). Among the mafic phases, ubiquitous clinopyroxene (Cpx) occurs in both crystal size classes; olivine (Ol) is present in some cases, either as phenocryst or in the groundmass. Ol phenocrysts can host Cr-spinel inclusions. Dark mica (phlogopite, Phl) can occur as deformed phenocrysts and/or microphenocrysts, while is always absent in the groundmass.

The sialic phases, which usually do not occur as phenocrysts, are represented by leucite (Lct), plagioclase (Plg) and alkali-feldspar (AlkF). The latter phase is

distinguishable in thin section as either millimeter-sized xenocrysts (i.e., characterized by rounded shape) or microphenocrysts in association with Lct. Otherwise, in the Plg-bearing scoria (see below) only the EDS spectra highlight the occurrence of AlkF, likely as high-temperature ternary feldspar (Di Luzio et al. 2018). Noteworthy, Lct and Plg did not crystallize together in the analyzed scoria clasts. This peculiarity allowed us to distinguish two groups of rock types: (1) Lct-bearing vs. (2) Plg-bearing scoria clasts.

In the Lct-bearing scoria clasts, Cpx, phlogopite (Phl) and melilite (Mel) phenocrysts and/or microphenocrysts show the most intriguing textural and microchemical features. Cpx crystals, up to 3 mm in size, have homogeneous, zoned or spongy texture, and range in composition from diopside to Al-rich diopside (Fig. 5a--i). Phl crystals are frequently characterized by kink bands, but rarely by thin oxide-bearing coronas, and show a wide range of $Mg/(Mg+Fe^{+2})$ ratio and relatively low Ti and F contents (Fig. 5c). The latter feature distinguishes Phl occurrences in scoria clasts with respect to lava flows (Boari et al. 2009). In some cases (GdR-4, SUP-2), Phl accompanies Ol in the phenocryst assemblage, while it does not occur when Ol is only present in the groundmass. In Mel-bearing scoria clasts (PAT-1), rare Phl is present as small, rounded microphenocrysts. In this case, Mel occurs in the groundmass or as microphenocrysts with elongated shapes that frequently host rounded Ol crystals (Fig. 5c).

The Plg-bearing scoria clasts are characterized by a simpler mineralogical assemblage ($Cpx+Plg\pm Ol\pm Mgt$) and relatively abundant fresh glass (Table 2). In this group, Cpx crystals, up to 1 mm in size, are relatively homogeneous and, interestingly, show a more constant composition (i.e., diopside content, $Mg/Mg+Fe^{2+}$) and a higher Al^{vi}/Al^{iv} ratio than in Lct-bearing scoria clasts (Fig. 4a-ii). Glasses are basaltic to trachybasaltic in composition in the Ol-bearing assemblage, while are phonotephritic in the Ol-lacking scoria clasts (see Supplementary material #3).

As specified above ("The Volsci Volcanic Field (VVF)"), in this paper, we refer to Lct- and Plg-bearing juvenile scoria clasts as HKS and KS rock types, respectively, for comparison to previous literature (Basilone and Civetta 1975; Civetta et al. 1979, 1981; Frezzotti et al. 2007; Boari et al. 2009).

$^{40}Ar/^{39}Ar$ data

New $^{40}Ar/^{39}Ar$ datings for the VVF eruptive products are reported in Table 3 and discussed in "New geochronologic constraints". Dating of phreatomagmatic products of the Roman Province is often challenging and results should be interpreted with caution (e.g., Marra et al. 2003, 2016). This is mainly due to xenocryst contamination owing to the widespread occurrence of accessory lithics (i.e., lava and pyroclastic fragments, hypo-abyssal granular rocks, loose crystals) entrained from diatreme-wall rock interaction (e.g., Valentine et al. 2015). Thus, the juvenile crystal fraction may occur even in subordinate proportion with respect to the xenocrystic ones. Furthermore, the juvenile component is often constituted of sub-aphyric scoria, lacking K-bearing phenocrysts suitable for dating.

Due to the sanidine-free erupted compositions of VVF phreatomagmatic centers, and since leucite in juvenile scoria is usually replaced by analcime (which would have resulted in significantly younger ages; Villa and Buettner 2009), in the present work, we dated loose crystals from the ash matrix of pyroclastic-surge deposits. Regarding age interpretation, it should be noted that the analyzed samples from phreatomagmatic deposits (SUP-1, GdR-1, PAT-1B, and PAT-5) yield significant age dispersion. However, these products were mainly sourced from isolated, monogenetic eruptive centers. Therefore, it is unlikely that the older age values might have derived from earlier buried volcanic edifices or erupted deposits, and yet may provide evidence of older magma batches that cooled in sub-surface conditions.

Thus, for those samples yielding scattered crystal populations, the eruption ages can be assessed based on the youngest populations of 4–5 crystals (Table 3, Fig. 6), which at least provide post-quem (maximum) age constraints.

In contrast, samples from Lct-bearing (HKS) scoria fall deposits, either from prevailing Strombolian activity (ARN-1) or from Strombolian phases associated with phreatomagmatic events (GdR-5, CLG), yielded homogeneous crystal populations and thus are reliable indicators of the eruption ages (Table 3, Fig. 6a, b).

Regarding KS products, the new $^{40}Ar/^{39}Ar$ data face the scarcity of suitable minerals for dating. For this reason, in the past, KS lavas were often dated on the groundmass (Boari et al. 2009), in which sparse alkali-rich feldspars are present (Civetta et al. 1979; Di Luzio et al. 2018). Similarly, we derived the ages of Plg-bearing scoria clasts (MOS-2, CA-C1, GdR-1, and POF-3) from few feldspar crystals (Table 3).

In example, sample POF-3 from scoria fall deposits yielded a homogeneous population of five crystals giving a weighted mean age of 397.7 ± 7.7 ka (Fig. 6a). A more precise weighted mean age of 393 ± 3.5 ka is obtained from the three youngest crystals. This age broadly matches that of the Colle Meringo Lct-bearing lava flow (390 ± 20 ka, Basilone and Civetta 1975), also related to the Pofi composite edifice, consistent with the lack of evidence in the field for intervening long time-breaks (e.g., testified by mature paleosoils). This points out that Plg-bearing and Lct-bearing magmas (KS and HKS, respectively) were erupting from the same eruptive source area in the same time range, as already noticed by Centamore et al. (2010) in this eastern sector of the VVF (i.e., Mola a Vento,

Table 2 Petrographic features of the VVF scoria clasts

Rock type	Sample	Eruptive center/unit	Macroscopic aspect	Microscopic aspect of juvenile scoria clasts			Matrix	Note
				Texture	Phenocrysts (> 500 μm)	Microphenocrysts and groundmass		
Lct-bearing (HKS)	PAT-1	Patrica NE	Clast-supported and consolidated	Porphyritic, scarcely vesicular, with scarce millimeter-sized phenocrysts (PI < 5) and relatively abundant microphenocrysts (< 500 μm)	Cpx + Ol	Cpx + dark mica + Lct + Mel + Mgt + scarce glass	Almost totally turned to calcite + chabazite, with abundant limestone lithics and scarce feldspar, dark mica and Cpx	Mel microphenocrysts are characterized by Ol inclusions. Rare microphenocrysts of dark mica show rounded shapes
	PAT-6	Patrica	Single scoria	Porphyritic (PI = 5–10), scarcely vesicular, with relatively abundant microphenocrysts (< 500 μm)	Cpx + Ol + Cr-spinel	Cpx + dark mica + Lct + Mgt + scarce glass		Rare microphenocrysts of dark mica are characterized by oxide rim or occurring as inclusions in Cpx
	POF-2	Pofi/Colle Marte unit	Single scoria	Porphyritic, moderately vesicular, with scarce millimeter-sized phenocrysts (PI < 5) and relatively abundant microphenocrysts (< 500 μm)	Cpx + Ol	Cpx + Ol + Lct + Mgt + scarce glass		Cpx characterized by sharp reverse zoning; abundance of fresh Lct microphenocrysts
	PZ4	Pofi/Mola a Vento unit	Single scoria	Porphyritic, moderately vesicular, with scarce millimeter-sized phenocrysts (PI < 5) and relatively abundant microphenocrysts (< 500 μm)	Cpx + Ol	Cpx + Ol + Lct + Mgt + scarce glass		Cpx characterized by sharp reverse zoning; abundance of fresh Lct microphenocrysts

Table 2 (continued)

Rock type	Sample	Eruptive center/unit	Macroscopic aspect	Microscopic aspect of juvenile scoria clasts			Matrix	Note
				Texture	Phenocrysts (> 500 μm)	Microphenocrysts and groundmass		
	GdR-4	Fosso di Monteacuto	Clast-supported and consolidated	Porphyritic (PI = 5–10), moderately vesicular, with relatively abundant microphenocrysts (< 500 μm)	Cpx + Ol + dark mica	Cpx + AlkF + Lct + Ap + glass	Almost totally turned in calcite + chabazite with abundant limestone lithics and feldspar, dark mica and Cpx	Occurrence of scarce AlkF microphenocrysts in scoria
	ARN-1	Arnara scoria cone	Clast-supported and consolidated	Porphyritic (PI = 5–10), moderately vesicular, with microphenocrysts (< 500 μm)	Cpx + dark mica	Cpx + dark mica + Lct + glass	Scarce matrix almost totally turned in calcite + chabazite	Presence of AlkF xenocrysts
	SUP-2	Supino	Matrix-supported and consolidated (peperino)	Porphyritic, moderately vesicular, with scarce millimeter-sized phenocrysts (PI < 5) and relatively abundant microphenocrysts (< 500 μm)	Cpx + Ol + dark mica	Cpx + Lct + Mgt + glass	Almost totally turned in calcite + chabazite with abundant limestone lithics and scarce sandstone	

Table 2 (continued)

Rock type	Sample	Eruptive center/unit	Macroscopic aspect	Microscopic aspect of juvenile scoria clasts			Matrix	Note
				Texture	Phenocrysts (> 500 μm)	Microphenocrysts and groundmass		
Plg-bearing (KS)	GdR-1	Villa S. Stefano	Matrix-supported and consolidated	Porphyritic, moderately vesicular, with scarce millimeter-sized phenocrysts (PI < 5) and relatively abundant microphenocrysts (< 500 μm)	Cpx + Ol	Cpx + Ol + Plg/AlkF + glass	Occurrence of olivine, Cpx, feldspar and dark mica in the matrix	The glass in scoria is almost totally turned to zeolite; rare unaltered glass in Ol-bearing glomeroporphyritic aggregate
	POF-3	Pofi	Matrix-supported and consolidated	Porphyritic (PI = 5–10), poorly vesicular, with relatively abundant microphenocrysts (< 500 mm)	Cpx + Ol	Cpx + Ol + Plg/AlkF + glass ±	Occurrence of sandstone lithics olivine, Cpx, feldspar, quartz and dark mica in the matrix	Xenocryst-rich matrix
	CA-C1	Ceprano–Colle Avarone	Clast-supported, unconsolidated and fines-poor	Porphyritic, moderately vesicular, with scarce millimeter-sized phenocrysts (PI < 5) and relatively abundant microphenocrysts (< 500 μm)	Cpx	Cpx + Plg/AlkF + Mgt + glass	Coarse Cpx, associated with feldspar, dark mica, amphibole and rare Lct-, dark mica-, feldspar-bearing lithics	Occurrence of K-rich accessory lithics

Table 3 $^{40}Ar/^{39}Ar$ ages of VVF eruptive products assessed on the youngest crystal population, except when indicated

Eruptive center/unit°	Sample #	Deposit type	Rock type	Lab	Dated material	Number of crystals	MSWD	Weighted mean age (ka) ± 2 σ
Colle Borello/UBO	MOS-2	Partially reworked, massive to laminated ash, with intervening scoria lapilli fall beds (base of UBO)	KS	B	Loose feldspar crystals in ash matrix	14 of 55	1.36	330.9 ± 2.6*
Villa S. Stefano	GdR-1	Massive, clast-supported beds of coarse ash and grey fine scoria lapilli, alternating with ash layers; bearing scarce leucite crystals and holocrystalline granular inclusions (italite); on top of *peperino*	KS	W	Loose feldspar and occasional leucite crystals in ash matrix	4 of 13	1.1	349.5 ± 5.0
Ceprano–Colle Avarone	CA-C1	Uppermost volcaniclastic horizon in Liri Basin lacustrine deposits: ca. 80-cm-thick, stratified, moderately lithified, clast-supported deposit of grey fine scoria lapilli, with scarce leucite and clinopyroxene crystals	KS	B	Loose feldspar crystals	8 of 28	0.82	345.4 ± 4.3
	CA-CGT	Volcaniclastic material in conglomerate (intermediate position in Liri Basin lacustrine deposits)	-	B	Loose feldspar and occasional leucite crystals in ash matrix	3 of 24	0.04	359.5 ± 6.5
Pofi–Colle La Grotta/ULG	CLG	Massive, slightly lithified, yellowish-brown, phreatomagmatic ash flow deposit, containing sparse leucite-bearing, black scoria clasts and sandstone blocks, and occasional accretionary lapilli and charred vegetable frustules; intervening "vesicular tuff" layers	HKS	B	Loose feldspar and rare leucite crystals in ash matrix	10 of 20	1.85	390.1 ± 3.6
Pofi scoria cone/POF_a	POF-3	Stratified succession of dark, fine scoria lapilli fall beds and grey ash layers, with occasional bomb sags; overlying a fallout deposit of black, highly vesicular scoria lapilli and spatter	KS	W	Loose feldspar crystals in ash matrix	3 of 5	1.2	393.0 ± 3.5
Arnara scoria cone/UAN_a	ARN-1	Scoria lapilli fall bed, enclosing arenaceous lithics, leucite and clinopyroxene free crystals	HKS	B	Loose feldspar and rare leucite crystals in ash matrix	5 of 20	0.46	394.5 ± 6.1
Supino	SUP-1	Partially reworked, stratified deposit of fine scoria lapilli beds, alternating with ash layers; analcime-bearing; on top of *peperino* remnants	HKS	W	Loose feldspar and leucite** crystals in ash matrix	4 of 22	1.0	406.2 ± 2.6
Patrica	PAT-5	Faintly bedded, greenish-brown, accretionary lapilli-bearing ash flow deposit underlying the basal erosional unconformity of *peperino*	HKS	W	Loose feldspar and rare leucite** crystals in ash matrix	3 of 21	0.32	541 ± 14.0

Table 3 (continued)

Eruptive center/unit°	Sample #	Deposit type	Rock type	Lab	Dated material	Number of crystals	MSWD	Weighted mean age (ka) ± 2 σ
Fosso di Monteacuto	GdR-5	Meter-thick, massive, clast-supported, reddish brown, lapilli tuff, made up of dark grey-purple fine scoria lapilli (occasionally cored), leucite, clinopyroxene and dark mica free crystals, arenaceous lithics, holocrystalline granular inclusions (italite); on top of *peperino*	HKS	W	Loose leucite crystals in ash matrix	17 of 21	1.0	742.5 ± 1.0
Patrica NE	PAT-1B	Massive to faintly laminated, light grey ash deposit (*peperino*), enclosing sub-mm scoria fragments, loose Lct and Cpx crystals, carbonate fragments	HKS	W	Loose leucite crystals in ash matrix	3 of 13	1.9	761.5 ± 9.5

All ages are calibrated according to ACs at 1.1848 ± 0.0006 Ma (Niespolo et al. 2017). Full analytical data are reported in Supplementary File #4A-B

B: $^{40}Ar/^{39}Ar$ single crystal fusion data the Berkeley Geochronology Center (BGC), California, U.S.A; W: $^{40}Ar/^{39}Ar$ single crystal fusion data WiscAr Laboratory, University of Wisconsin–Madison, USA; *MSWD* mean standard weighted deviation

*Oldest crystal population

**Occurring as xenocryst

°For unit labels of eruptive centers cf. Centamore et al. (2010). The relatively low/medium-K (KS) vs. high-K (HKS) nature is also indicated

Arnara). We note that the age of 298 ± 28 ka obtained by Boari et al. (2009) for a KS lava flow of the Pofi edifice, interbedded between the Fosso Meringo lava plateau and the fallout deposit of the POF_a unit (sample POF-3), is stratigraphically inconsistent with the age of ca. 390 ka of the bracketing units.

Regarding the apparently problematic age of sample MOS-2, which yielded a statistically consistent older population of crystals with a weighted mean age of 330.9 ± 2.6 ka ($n = 14$), along with a number of scattered crystal ages as young as 12 ka (Fig. 6b), this is likely the result of the deep weathering that affected this deposit (see Suppl. Material #1). Indeed, the low %Ar* of most of young crystals suggests a possible Ar loss due to deep alteration, which is one potential cause for age rejuvenation. Indeed, when a cutoff at %Ar* < 50 is applied, only two, statistically poorly significant younger crystals are left. Notably, the age of 331.6 ± 3 ka that we attribute to MOS-2 is the youngest in our dataset, consistent with the inferred stratigraphic position of the Colle Borello unit on top of the local VVF successions (UBO; Centamore et al. 2010).

Discussion

Constraints to the VVF pre-eruptive magma system

The Lct-bearing scoria clasts of the VVF (HKS rock type, Table 2) originated from high-K parental magmas, similar to the Middle Latin Valley volcanics described in literature as high-K rocks or as HK series (Boari et al. 2007, 2009; Frezzotti et al. 2007). The wide range of $Mg/(Mg + Fe^{2+})$ values for Cpx and Phl phenocrysts in Lct-bearing scoria clasts indicates that parental magmas underwent significant pre-eruptive crystallization, as also suggested by the MgO contents (3.62–6.55 wt%) reported in literature, mainly for HKS lava flows (Boari et al. 2007, 2009; Frezzotti et al. 2007). In particular, the textural features of the Lct-bearing scoria clasts hosting Mel (PAT-1, Patrica NE center) suggest that the early erupted magmas of VVF originated from a fractional crystallization process coupled with the assimilation of carbonate wall rocks of the Volsci Range. In fact, rounded Ol inclusions in Mel microphenocrysts (Fig. 5) indicate that Ol was not stable in paragenesis with Mel, and that the latter formed by a reaction between Ol and a melt enriched in calcium via the assimilation of sedimentary carbonate. This process is in agreement with the phase relationships in the system Forsterite–Diopside–Akermanite–Leucite at low pressure (Gupta 1972) where at the thermal minimum occurs an olivine-free assemblage, constituted by clinopyroxene + akermanite (i.e., melilite) + leucite + melt. Also, high (> 6.4‰)

Fig. 4 Field aspects of representative volcanic deposits at the outcrop and sample scales. **a**, **e**, **f** Alternating base surge ash deposits and scoria lapilli fallout layers; **b** accretionary lapilli-bearing ash; **c** "peperino" facies; **d** strongly lithified, well-sorted, fine scoria lapilli, with pervasive interstitial calcite

$\delta^{18}O$ values of Cpx in the Mel-bearing lava of Colle Castellone (Frezzotti et al. 2007) point towards the interaction of the early high-K magmas with sedimentary carbonate (cf. Gaeta et al. 2006; Di Rocco et al. 2012). Here, we do not attempt to model mathematically the carbonate AFC process at the origin of the Mel-bearing rocks of VVF, as the end-member representing the parental magma is, currently, not well constrained isotopically. So far, the temporal change in the radiogenic isotopes of parental magmas has been defined for the Colli Albani and Sabatini major ultrapotassic districts of the Roman Province (i.e., $^{87}Sr/^{86}Sr$ trend from ~ 0.711 to 0.709 with time; Gaeta et al. 2006, 2016; Sottili et al. 2019), but not for VVF.

Except for the early VVF activity, carbonate assimilation was less extensive than at Colli Albani, as indicated by the scarcity of low-silica, K-foiditic rocks and the lower F content of Phl in VVF Lct-bearing scoria clasts in comparison to Colli Albani (Gaeta et al. 2000). In fact, the activity of F in Phl inversely correlates with the activity of H_2O in the magma that, in turn, inversely correlates with that of CO_2. Different from Colli Albani (cf. Freda et al. 2008), the relatively low F content of Phl indicates a low

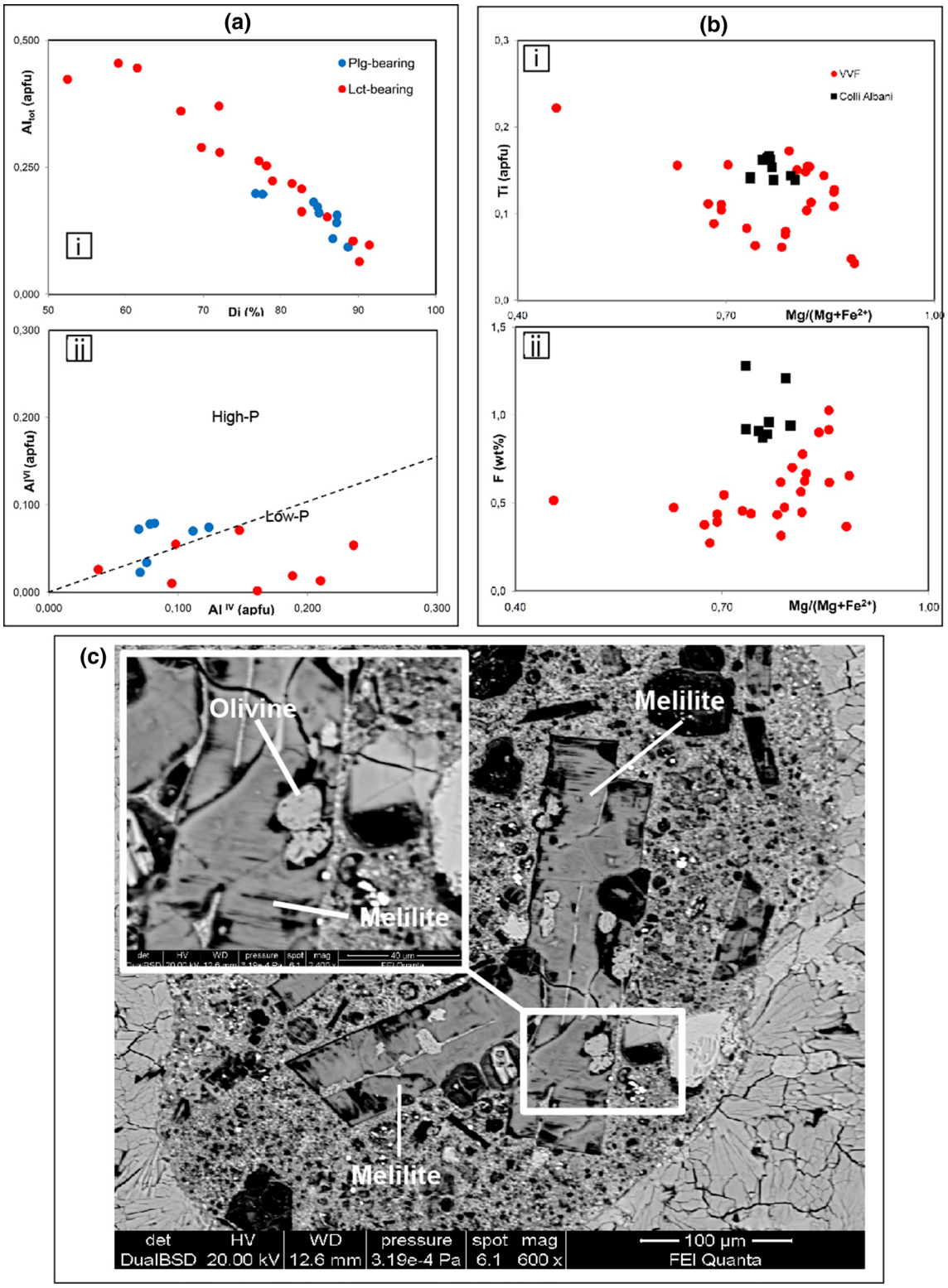

Fig. 5 **a** Clinopyroxene chemical compositions from the two groups of VVF rock types, reported in the Al_{tot}-Di (upper) and Al^{IV}–Al^{VI} (lower) diagrams. The dashed line in the latter plot is an arbitrary limit between high ($p \geq 0.4$ GPa) and low ($p \leq 0.4$ GPa) pressure clinopyroxenes, based on experimental results at high pressure (Perinelli et al. 2019). **b** Phlogopite chemical compositions from VVF (this work) and Colli Albani (data from Gaeta et al. 2000) rock types, reported in the Ti–Mg/(Mg + Fe^{2+}) (upper) and F–Mg/(Mg + Fe^{2+}) (lower) diagrams. **c** SEM Electron backscattered image of a Lct-bearing scoria (sample PAT-1) containing melilite. The latter mineralogical phase occurs as microphenocrysts with elongated shape, hosting rounded olivine crystals (inset)

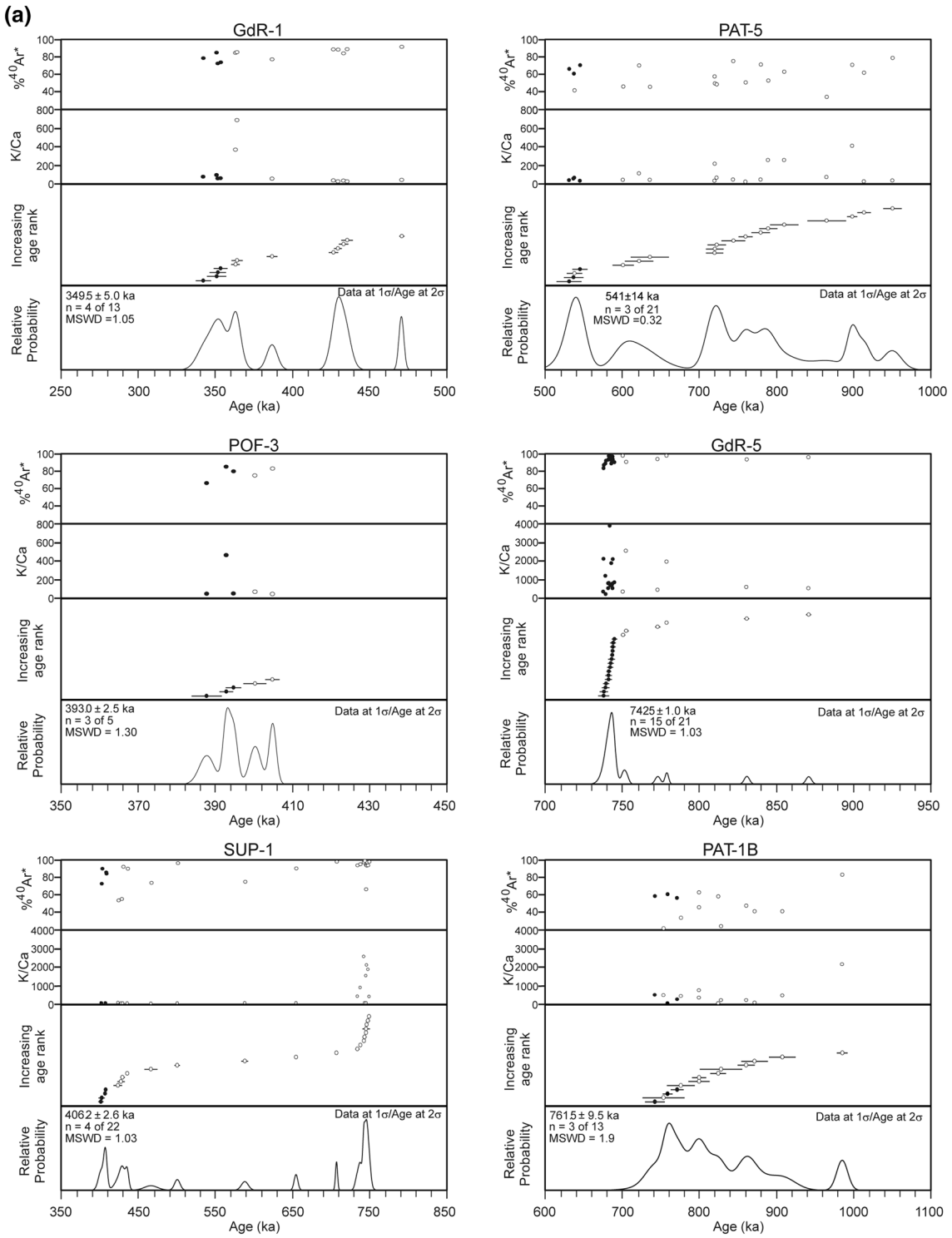

Fig. 6 $^{40}Ar/^{39}Ar$ results for the samples analyzed at WiscAr (**a**) and at BGC (**b**). For each sample, the plots show (from the top to bottom panels) the percent radiogenic ^{40}Ar ($^{40}Ar^{*}$), K/Ca ratios (derived from ^{39}Ar and ^{37}Ar measurements), $^{40}Ar/^{39}Ar$ ages of feldspar and/or leucite from single grain analyses, and associated probability distribution functions. Weighted mean ages (reported with 2σ uncertainties) are assigned when distinct populations can be detected and interpreted in light of age data and field context. To avoid additional complications in data interpretation imposed by $^{40}Ar/^{39}Ar$ dates with low radiogenic ^{40}Ar yields, all crystals with < 50% Ar* are not considered for weighted mean age calculations. Open circles: data not included in the weighted mean. See text for detailed interpretations

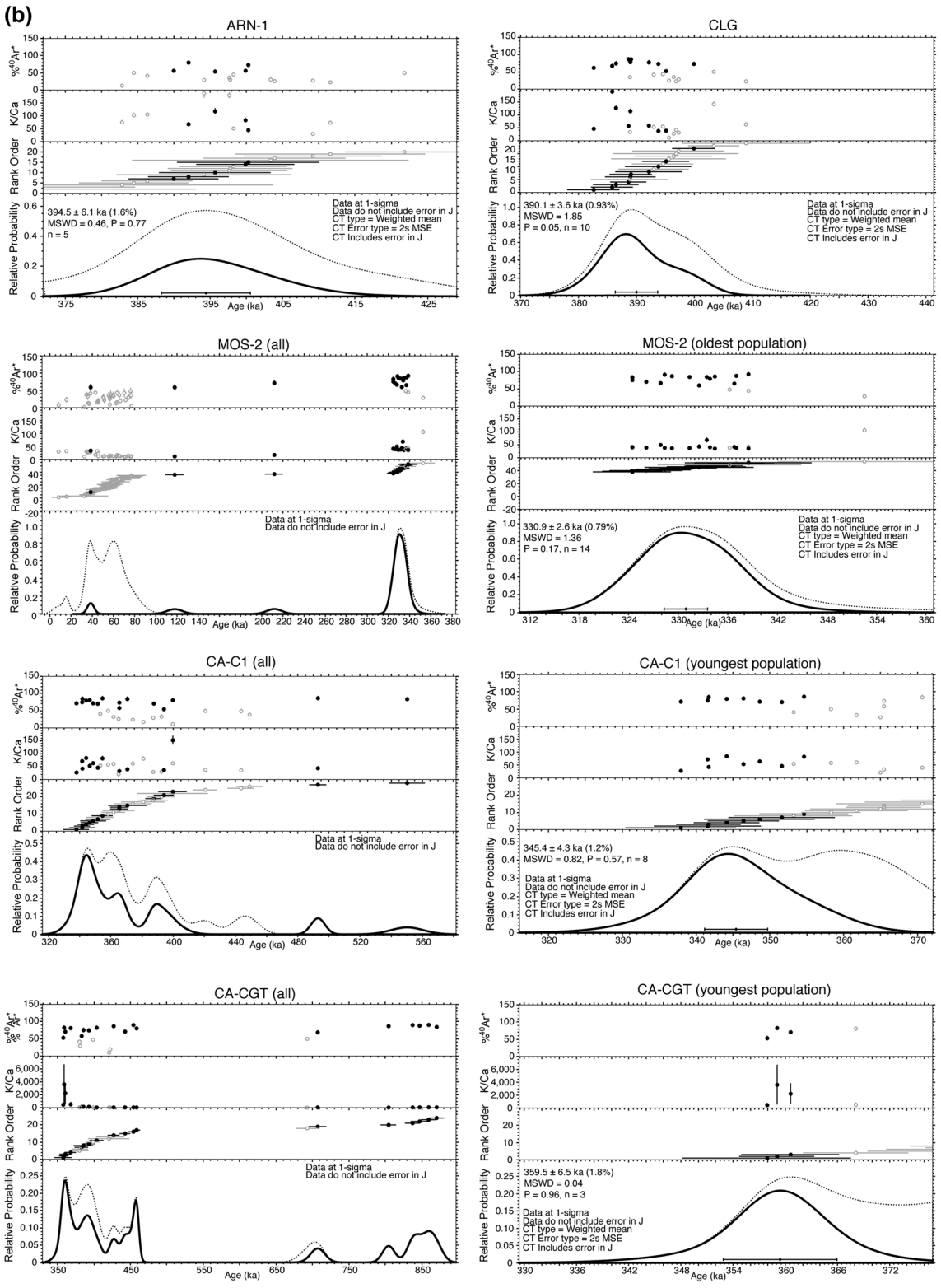

Fig. 6 (continued)

CO_2 activity in the VVF magma system, which allowed an early and more prolonged presence of Phl on the magma liquidus. In addition, the higher values and wider range of Mg# of VVF Phl with respect to Colli Albani (Fig. 5b) consistently indicates a wider Phl stability field in the VVF magma system. This explains the observed association of Phl with Ol in the phenocryst assemblage of VVF Lct-bearing scoria clasts, which, instead, is lacking in the Colli Albani scoria clasts (e.g., Freda et al. 1997, 2006, 2011; Palladino et al. 2001; Marra et al. 2009; Gozzi et al. 2013; Gaeta et al. 2016). An early and prolonged Phl crystallization should profoundly affect the trace element abundance in magmas. Coincidentally, the VVF magmas show a wide range in Rb content, which spans over more than one order of magnitude, with nearly constant composition of the other geochemical parameters (Frezzotti et al. 2007).

We note that in the Phl-bearing HKS examples (i.e., GdR-4, ARN-1, and SUP-2; Table 2), Lct is absent among phenocrysts, whereas it occurs as microphenocrysts. Consistently, a relatively wide Phl stability field provides evidence for an origin from a deep, hydrated magma reservoir in which Lct was not stable, so that Lct crystallization took place at relatively shallow depth in the eruption feeder system. Noteworthy, in other cases where high-K magmas are represented by Lct-bearing, Phl-free scoria clasts containing Ol in the groundmass (i.e., samples PZ4 and POF-2; Table 2), the lack of Phl crystallization indicates a shorter residence time in the plumbing system, in agreement with the primitive magma composition (MgO ≈ 10 wt%; Centamore et al. 2010).

The Plg-bearing scoria clasts of the VVF originated from a low/medium-K parental magma (here referred to as KS), similar to the Middle Latin Valley volcanics described in literature as calc-alkaline or shoshonitic rocks (Boari et al. 2007, 2009; Frezzotti et al. 2007). Plg-bearing scoria clasts lack Phl and contain Cpx phenocrysts with a narrow compositional range with respect to Lct-bearing scoria clasts (Fig. 4a). The limited chemical evolution of Cpx thus suggests a shorter sub-surface residence time of magmas, also in agreement with the experimental growth rate (Bonechi et al. 2020): in fact, Cpx phenocrysts are finer (max. 1 mm in size) in Plg-bearing scoria clasts than in Lct-bearing ones (up to 3 mm). Moreover, the higher Al^{vi}/Al^{iv} ratio for Cpx in Plg-bearing scoria clasts than in Lct-bearing ones (Fig. 5a) indicates a higher pressure of crystallization for the KS parental magma. This has recently been tested experimentally (Perinelli et al. 2019) using a primitive K-basalt from Procida Island (Campi Flegrei) similar to the primitive KS rocks of VVF in composition (Frezzotti et al. 2007). In the VVF, Plg-bearing scoria clasts, containing small, poorly differentiated, high-pressure Cpx, derived by primitive, low/medium-K parental magmas, thus strongly suggest a fast ascent from a deeper reservoir with respect to the slightly differentiated, high-K, Lct-bearing magmas.

New geochronologic constraints

Eleven new age determinations, integrated with the existing 21 ages selected from the literature (Basilone and Civetta 1975; Boari et al. 2009; Centamore et al. 2010), allow us to depict an overall eruptive history for the VVF, spanning from 761.5 ± 9.5 ka (this work) to 231 ± 19 ka (Centamore et al. 2010). Moreover, we are now able to outline the migration of the eruptive centers in space and time (Fig. 2ai–iii) with respect to the erupted magma compositions.

Xenocryst populations (either from local or distal sources) occurring in the dated phreatomagmatic products provide insights into the onset of potassic magmatism since at least 1206 ± 40 ka (weighted mean age of two feldspar crystals; sample PAT-5; Figure S1 and Table S1 in Supplementary File #5). Moreover, the crystal age spectrum from gravelly deposits at Colle Avarone (sample CA-CGT, Fig. 6b), on top of the sedimentary fill of the Liri Basin yielded old ages at ca. 870–820 and 700 ka.

Following this poorly constrained paleo-magmatism of uncertain source, three major phases of activity can be defined at VVF, whose age ranges and related uncertainties are imposed directly from the interpreted $^{40}Ar/^{39}Ar$ ages:

1. "Early eruptive phase" (761.5 ± 9.5 – 539.3 ± 11 ka), defined by the oldest and youngest dated product sourced in the carbonate Volsci Range backbone (i.e., the Patrica NE and the Fosso di Monteacuto centers). In particular, the Patrica, Patrica NE and Piglione (614 ± 10 ka; Boari et al. 2009) centers lie along a NW–SE volcano-tectonic lineament, a segment of the NW-trending fault system bounding the Volsci Range and the Middle Latin Valley Graben. Moreover, the Colle Castellone center (600 ± 4 ka; Boari et al. 2009) developed along the southern segment of the same fault, bordering the Middle Latin Valley Graben (Fig. 2). Phreatomagmatic deposits, characterized by the typical peperino facies rich in carbonate lithic inclusions, as well as the Piglione and Colle Castellone lava occurrences, are HKS, Lct + Mel-bearing rock types, which consistently indicate a significant degree of magma–wall rock interaction.
2. "Main (Climactic) Eruptive Phase" (424 ± 13–349.5 ± 5.0 ka), comprised between the Lower Tomacella unit (Boari et al. 2009) and the Villa S. Stefano center (this work), extending to 330.9 ± 2.63 ka (Colle Borello, MOS-2, this work). The source areas of the VVF climactic activity clustered along a NNE-trending volcano-tectonic lineament (i.e., Tecchiena, Selva dei Muli, Tomacella, Celleta, Giuliano di Roma; Fig. 3) and

in the Pofi area (i.e., Arnara and the Pofi polygenetic center, also including major effusive activity of Fosso Meringo lava flow). At a larger scale, the Pofi source area may represent the eastern termination of an ENE-trending belt of volcanic centers extending to the west across the early Fosso di Monteacuto center, as far as the Pontina Plain at the VVF periphery (Fig. 1). This time span also includes the ages of the distal products in the southeastern reach of the Liri Basin (402 ± 5 to 351 ± 3 ka; Nomade et al. 2011; Pereira et al. 2018);

3. "Late Eruptive Phase" (300 ± 28 to 231 ± 19 ka?), concentrated within the Sacco River Valley. In particular, several volcanic centers (e.g., Colle Vescovo, Colle Sant'Arcangelo, Colle Celleta, Colle Spinazzeta) developed along the major NW-trending fault system bounding the Middle Latin Valley graben, i.e., the same fault system that controlled the early phase of activity (e.g., Colle Castellone).

VVF eruptive history

Overall, the VVF eruptive pattern was characterized by small volume (in the order of 0.01–0.1 km^3, based on an approximate estimation of the mapped deposits) eruptions from a network of monogenetic centers, totaling nearly 4 km^3 (i.e., two orders of magnitude lower than the major potassic volcanic districts of the Roman province). Available geochronological constraints suggest that long quiescence periods (in the order of 10^5 years) occurred between isolated eruptive events during the early activity phase (since ca. 760 ka), which was followed by a climactic eruptive activity clustered at around 0.4 Ma in the eastern sector of VVF (with a tail possibly extending up to 0.2 Ma). Early activity was essentially fed by K-rich, Lct + Mel-bearing magmas, showing evidence of relatively high degree of carbonate assimilation, possibly due to multi-stage ascent through thick carbonate successions (hence the diffuse phreatomagmatic character).

Subsequently, during the main activity phase in the eastern VVF sector (since ca. 420 ka), HKS rock types alternated with poorly differentiated, Plg-bearing KS rock types from eruptive sources close in time and space (e.g., Ceccano and Pofi areas). In particular, the eruptive activity along the major faults bounding the Middle Latin Valley Graben (e.g., Colle del Vescovo, Selva Piana, and Colle Capirolo centers) testifies for the fast ascent of nearly primary KS magmas (K-basaltic in composition; Centamore et al. 2010).

The actual duration of the most recent activity in the VVF remains an open question, due to the analytical uncertainties of the existing K–Ar age determinations and the analytical errors associated with the re-calculated $^{40}Ar/^{39}Ar$ ages from Boari et al. (2009), as well as with those reported in Centamore et al. (2010) (Table 1). The youngest age reported in Boari et al. (2009) refers to the Colle Sant'Arcangelo Lct-bearing lava (ERN 86, 254 ± 4 ka). However, despite the small error, this age relies only on the four first steps with K/Ca ratios > 100, whereas the other steps display K/Ca < 70, suggesting that either a dishomogenous mineral assemblage was involved in the dated lava groundmass, or pervasive analcimization of Lct caused a rejuvenation of the age. We remark that, if this age value is correct, the HKS lava of Colle Sant'Arcangelo would be the youngest dated product in Boari et al. (2009), and younger than any KS products dated in the present work, in conflict with the petrologic evolution suggested by Boari et al. (2009), according which KS magmas were the last erupted.

In addition, two KS lava flow samples yielded groundmass plateau ages with low precision: the age of 302 ± 28 ka obtained for ERN 94 (Colle Vescovo) relied only on 4 steps and included only 66% of the total $^{39}Ar_K$; the age of 289 ± 32 for ERN100 (Pofi volcano) is more robust, including 100% of the $^{39}Ar_K$, although incongruent with the age of 393.0 ± 3.5 ka that we obtained for Plg-bearing activity at Pofi (POF-3).

Finally, we cannot fully evaluate the consistency of the two $^{40}Ar/^{39}Ar$ ages age determinations of 263 ± 58 ka (Colle Capirolo) and 231 ± 19 ka (MVN unit of Pofi volcano) reported in Centamore et al. (2010), due to the lack of full analytical details. New dating efforts are thus needed to assess the actual timing of the late phase of activity at VVF.

Insights on magma source

New data presented in this paper show that the eruption of high-K (Lct-bearing) and lower-K (Plg-bearing and Lct-free) magmas was broadly concomitant during the VVF activity, which puts constraints on the geometry of the metasomatic mantle source. The most primitive, KS magmas of the VVF were likely saturated by amphibole (Amph) at high pressure, as supported by experiments on analogue compositions, in which Phl saturation was never achieved (Perinelli et al. 2019; Bonechi et al. 2017). It is worth noting here that the most primitive high-K magmas of the Roman Province are instead saturated by Phl at high pressure (Conte et al. 2009). On these grounds, the observed temporal shift from HKS to KS magmas at VVF cannot be explained in the frame of a laterally heterogeneous, veined mantle. It would imply the exhaustion of a Phl-bearing vein (source of HKS magmas) prior to an Amph-bearing one (source of KS magmas), which would conflict with the higher melting temperature of a Phl-bearing mantle source with respect to an Amph-bearing one. Alternatively, different depths of mantle partial melting could be at the origin of HKS vs. KS parental magmas (e.g., Frezzotti et al. 2007; Peccerillo 2017). In our view, consistent with Cpx barometric constraints (Fig. 5), a vertically zoned metasomatized mantle

would imply a shallower and older Phl-bearing layer (e.g., Gaeta et al. 2016), and a deeper Amph-bearing layer related to Cenozoic subduction dynamics. The late onset of KS magmatism at VVF may indicate the partial melting of the Amph-bearing layer at higher pressure with respect to the Phl-bearing source of early activity. An increasing extensional rate (possibly linked to the dynamics of the subducting slab, see below) would have resulted in an enhanced degree of decompression, allowing a deeper source melting and the production of KS magmas.

Volcano-tectonic relationships

Chronostratigraphic indications show that > 80 m-thick fluvial-lacustrine sediments accumulated in the Liri Basin in the time span 600–350 ka (Fig. 3), constraining the timing of tectonic subsidence of this sector of the Latin Valley. The structural setting of the area (Fig. 1) shows a marked control of the NW-striking normal faults on the geometry of the Liri Basin, which was affected by NE–SW oriented extensional tectonics coeval with the widespread Middle Pleistocene tectonics forming the intramountain basins of central Apennines (Cosentino et al. 2017 and references therein). Phases of coupled major extensional tectonics and volcanic activity have been evidenced for the volcanic districts of the Tyrrhenian Sea margin of central Italy (e.g., Acocella and Funiciello 2002; Marra et al. 2004; Marra and Florindo 2014). Here, we outline the timing and structural control on magma ascent at VVF.

The major NW-striking normal fault system bounding the Volsci Range and the Middle Latin Valley Graben (Fig. 1) controlled the location of early activity centers sourced in the carbonate substrate (i.e., Patrica NE, Piglione, Colle Castellone; ca. 761–604 ka), as well as the alignment of late eruptive centers (i.e., Colle Vescovo, Colle Sant'Arcangelo, Colle Celleta, Colle Spinazzeta; possibly up to ca. 250 ka). This NW-trending volcano-tectonic lineament may be essentially related to the upper crust (< 12–15 km depth) fault architecture dominated by Quaternary extensional structures and older re-activated faults.

Instead, the NNE-trending (Tecchiena, Selva dei Muli, Tomacella, Celleta, Giuliano di Roma) and ENE-trending Ceccano Fault (Ceccano and Pofi source areas) volcano-tectonic lineaments controlled the cluster of eruptive centers during the VVF climactic activity (ca. 424–349 ka). While the ENE-trend is an expression of a broader (in space and time) lineament extending to the western VVF periphery as far as the Pontina Plain, the activity of the NNE-trend was more focused in time. These lineaments might be related to high-angle faults with strike-slip kinematics (e.g., Sani et al. 2004), which may represent the surface expression of deeper slab-mantle dynamics and the preferential pathways for magma injection into the crust (Acocella et al. 1996; Centamore et al. 2010; see "Volcano-tectonic relationships"). The re-activation of high-angle lithospheric faults in the extensional regime that affects the inner Apennines since at least Pleistocene may potentially tap magma deeper than the typical NW-striking normal faults of the Apennines that cross-cut limitedly the upper crust, thus driving the emission of primitive magmas (Acocella et al. 1996; Acocella and Funiciello 2002, 2006). As a result, crustal-scale dilational jogs may form at depth, whose surface expression is the dextral wrench zone cutting across the Volsci Range, shaping the Middle Amaseno and Middle Latin valleys. In this frame, the reported 400–351 ka volcaniclastic occurrences within the sedimentary fill of the Liri Basin (Nomade et al. 2011; Pereira et al. 2018) indicate that the tectonic phase responsible for this graben-like tectonic structure was coeval with the climactic phase of activity in the VVF.

The analysis of the instrumental seismicity in the years 2009–2019 highlights the occurrence of sparse seismicity in the Latin Valley, as opposed to the high concentration of moderate to strong events within the main Apennine chain (Fig. 5). This indicates low deformation rates within the Latin Valley, where focal mechanisms account for the re-activation, besides dip-slip NW-striking faults, of NNE-striking faults with oblique-slip kinematics, consistent with a prevailing NE-oriented σ_3, as typical of the Apennines (Montone and Mariucci 2016).

The role of the NNE-trending lineaments in controlling the pathways of volcanic activity has been shown in this paper not to be exclusive, but accompanying the NW- and ENE-oriented alignments of eruptive centers. We interpret the NNE- and ENE-trending lineaments to have been re-activated under the NE-oriented extensional regime affecting the upper crust during the VVF activity time span.

Geodynamic implications

The peculiarities of the VVF with respect to the other potassic volcanic districts of the Tyrrhenian Sea margin of central Italy, despite the common temporal range of activity, are summarized as follows: (1) the small volume of total erupted products (in the order of a few vs. hundreds of km^3); (2) the low intensity and magnitude of individual eruptive events vs. large Plinian and/or caldera-forming eruptions; (3) the lack of highly differentiated rock types, which indicates rapid magma ascent from the mantle source, with limited stationing in shallow magma chambers; (4) the coexistence of both HKS and KS primitive magmas (in some ways, similar to Roccamonfina volcano nearby) that usually characterize distinct volcanic districts (e.g., HKS at Somma-Vesuvius vs. KS at Campi Flegrei).

Overall, the paucity of erupted magma at VVF would suggest low degree of partial melting of the mantle source and/or hindered ascent to surface. Lct-bearing (HKS) and

Lct-free (KS) magmas characterized distinct eruptive phases and/or eruptive centers, although with some spatial and temporal superposition, yet with no evidence of pre-eruptive mixing/mingling. HKS magmas mostly fed the early phase of activity (sourced in the Volsci Range setting), then KS magmas appeared during the climactic phase, partially overlapping in time and space with HKS ones (e.g., in the Pofi–Ceccano areas); KS magmas prevailed during the late phase of activity, although still accompanied by HKS events.

We note that the eruption of Lct-bearing products (from slightly differentiated HKS magmas), in particular those containing Phl, requires some prolonged pre-eruptive magma stationing and/or multi-stage ascent through carbonate rocks in diatreme systems (Cardello et al. 2020). In contrast, Plg-bearing eruptive products (from poorly differentiated KS magmas) reflect fast ascending primitive magma batches allowing "bullet eruptions". Below, we propose that such a change in the magma plumbing system may have resulted from an acceleration in the extensional rate affecting the upper plate associated with the slab retreat.

The eruption of primitive magmas at VVF (mostly in the 420–230 ka time span) from volcanic centers clustered along regional high-angle faults of lithospheric depth suggests a link to the geodynamic setting of the central sector of the Apennines. This is characterized by the differential retreat of the W-directed subducting Adriatic plate between the northern arc of the Apennines (associated with the Middle–Upper Pleistocene potassic magmatism of the Roman Province) and the southern arc related to Campanian magmatism, also including the presently active Ischia, Campi Flegrei and Somma–Vesuvius volcanoes. In the context of the Africa–Europe convergence, the Tyrrhenian basin–Apenninic arc system (Malinverno and Ryan 1986) formed as a result of the evolution of the accretionary prism characterizing the upper plate. Patacca and Scandone (1989) recognized the progressive development of two distinct (i.e., northern and southern Apennine) arcs of subduction in the post-Tortonian times. Slab retreat triggered the extensional regime presently characterizing the Tyrrhenian Sea margin of Italy (Malinverno and Ryan 1986; Patacca and Scandone 1989), which, otherwise, would not have occurred in the compressive domain of the Africa–Europe convergence. Thus, the mainly compressive stress field acting at depth is accompanied by an extensional regime in the upper crust, associated with the gravity spreading of the Apennine chain (Fig. 7), which may provide preferential pathways to magma uprising.

Several authors, based on tomographic datasets, claimed for a lateral discontinuity in the subducting plate below the Apennines. For instance, Spakman (1991) and Spakman et al. (1993) suggested the occurrence of a slab detachment below the central-southern Apennine. Lucente and Speranza (2001), through teleseismic tomography, noticed the lack of high velocity anomalies in the depth range 35–100 km in the Apennine sector confined between the Ancona–Anzio and the Ortona–Roccamonfina lines (Fig. 7). Compared to the continuous high velocity zone existing in the 340–440 km depth range, mirroring the shape of the whole Apennine chain from northern Tuscany to Calabria, this tomographic discontinuity was attributed to a local slab detachment and cessation of subduction. Recent tomographic investigations have demonstrated a segmented geometry of the subducting slab (Ascione et al. 2012; Giacomuzzi et al. 2012; Chiarabba et al. 2014; Rosenbaum and Piana Agostinetti 2015; Chiarabba and Palano 2017). In particular, based on the upper mantle structural frame of Rosenbaum et al. (2008), Rosenbaum and Piana Agostinetti (2015) suggested a link between the asthenospheric-derived magmatism and the "central Apennine slab window", regarded as the expression of advanced slab tearing (Pierantoni et al. 2020).

The origin of VVF magmas has been attributed to a variably metasomatized, heterogeneous mantle source, although the timing of the metasomatic processes and the geometry of heterogeneity (i.e., lateral veins vs. vertical layering) are still debated (Boari et al. 2009; Conticelli et al. 2009; Nikogosian and van Bergen 2010; Gaeta et al. 2016; Kornneef et al. 2019). In this context, the eastward migration of the southern segment of the subducting plate (between approx. 6 and 2 Ma; Rosenbaum et al. 2008) may have produced a subduction gap (i.e., a central Apennine slab window), thus shifting away from the VVF-hosting area a potential source of volatiles required for the partial melting of the metasomatized mantle, and limiting the degree of partial melting. Conversely, the presence of a subducting slab underneath the nearby major volcanic districts of the Roman and Campanian provinces ensured volatile transfer to the mantle source and extensive magma production from Middle Pleistocene to present.

This scenario would explain the very limited amount of erupted products at VVF, despite the availability of easy ascent pathways (testified by small-scale, bullet eruptions fed by primitive magmas), as the consequence of very limited production of magma (rather than hindered ascent that would have resulted in extensive plutonism). This is typical of tectonically controlled volcanic fields (Valentine and Perry 2007), where melt generation is dependent on tectonic forces, and the very low magma flux is a passive byproduct of regional tectonic strain.

We also suggest that, while the retreat of the lower plate affected dramatically the productivity of the mantle source, the re-activation of structural lineaments in the upper plate favored the ascent and eruption of very small batches of poorly to slightly differentiated magmas. In particular, the observed compositional shift from HKS to KS primitive magmas during the VVF activity climax was concomitant to enhanced mantle decompression. In our view, this may be

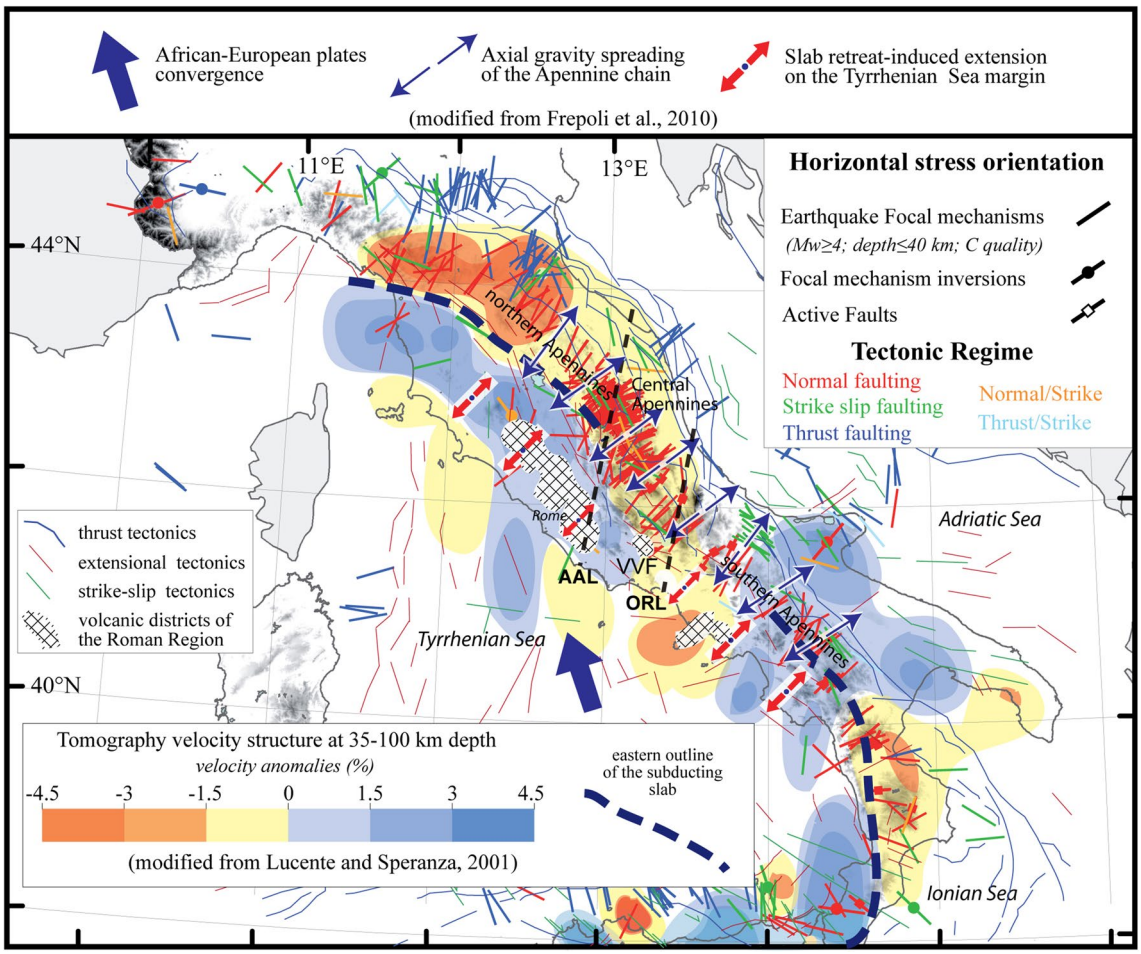

Fig. 7 Sketch geodynamic overview of peninsular Italy. Present day stress map, along with the main tectonic features, modified from Montone and Mariucci (2016) and Mariucci and Montone (2019). The horizontal stress orientations correspond to σ_3, for normal and normal/strike faulting tectonic regime, and to σ_1 for strike-slip, thrust and thrust/strike faulting. Tomography of the region modified from Lucente and Speranza (2001). Geodynamic vectors modified from Frepoli et al. (2010), based on Faccenna et al. (1996). *AAL* Ancona–Anzio line, *ORL* Ortona–Roccamonfina line, *VVF* Volsci Volcanic Field

due to an increase in the extensional rate in the upper plate (possibly related to an increasing rate in the slab retreat), also responsible for the rapid subsidence of the Liri Basin.

As a whole, in response to changing degrees of decompression, mantle melting was localized in small-scale domains, producing small magma batches, their ascent being favored by enhanced crust permeability due to major fault interconnection.

Summary

Through a set of 11 new $^{40}Ar/^{39}Ar$ age determinations, we have implemented the reconstruction of the eruptive history of the VVF. Integrated geochronological data and field observations allow us to outline three major phases of activity:

1. Early Eruptive Phase (761.5 ± 9.5 to 541.0 ± 14 ka);
2. Main (Climactic) Eruptive Phase (424 ± 13 to 349.5 ± 5.0 ka);
3. Late Eruptive Phase (300 ± 28 to 231 ± 19 ka?).

Long quiescence periods occurred between isolated eruptive events from ca. 0.8 to 0.4 Ma, whereas a climactic eruptive activity clustered at around 0.4 Ma. The age of the most recent activity in the VVF remains an open question and new dating efforts are still in order.

The VVF is an example of a tectonically controlled volcanic field. Eruptive centers, mostly monogenetic tuff rings and scoria cones with lava occurrences, appear to be aligned along the main NW–SE border fault of the Sacco River Valley (separating the Middle Latin Valley Graben and the Volsci Range settings), as well as along "transversal" NNE- and ENE-trending lineaments.

Several peculiarities characterized the VVF with respect to the other volcanic districts of central Italy:

1. the small volume of total erupted products from a network of monogenetic centers, as opposed to high-volume eruptions from large central or areal volcanoes;
2. the low intensity and magnitude of individual eruptive events;
3. the lack of highly differentiated rock types, which indicates fast magma ascent from the mantle source;
4. the coexistence of both Lct-bearing (HKS) and Plg-bearing (KS) primitive magmas. In particular, HKS magmas fed the early phase of activity, then KS magmas appeared during the climactic phase, partially overlapping in space and time with HKS ones, and then prevailed during the late phase of activity.

In our interpretation, the differential retreat of the segmented W-directed subducting Adriatic plate (at about 6–2 Ma), resulting in lateral slab tear (central Apennine slab window), shifted away a potential source of volatiles from the heterogeneous metasomatized mantle source beneath VVF, thus limiting the degree of partial melting and magma production. During the Quaternary, the dominant compressive stress field acting at depth was accompanied by an extensional regime in the upper crust, associated with the gravity spreading of the Apennine chain, allowing the fast ascent of small, primitive magma batches through re-activated high-angle faults of lithospheric depth.

These factors may explain:

1. ascent and eruption of very small batches of magmas, favored by the re-activation of structural lineaments in the upper plate during the 800–400 ka interval;
2. increase in the extensional rate in the upper plate, possibly related to an increasing rate in the slab retreat, during the 400–350 ka interval;
3. enhanced subsidence of the Liri Basin, broadly coeval with the VVF eruptive climax;
4. enhanced mantle decompression producing the observed compositional change toward KS primitive magmas during the VVF activity climax;

Our results set the groundwork for addressing geodynamic questions concerning the timing and significance of the processes affecting the upper plate, e.g., lateral slab tear, and slab break-off.

Supplementary Information The online version contains supplementary material available at https://doi.org/10.1007/s00531-021-01981-6.

Funding Open Access funding provided by Istituto Nazionale di Geofisica e Vulcanologia. This research did not receive any external funding.

Compliance with ethical standards

Conflict of interest The authors declare no conflict of interest/competing interests.

Availability of data and material Data archiving is underway and will be openly available in PANGAEA (https://www.pangaea.de/). For review purposes, we uploaded our data as Supporting Information.

References

Accordi B, Segre AO, Cocozza T, Angelucci A, Sirna G, Farinacci A (1966) Sheet 159 Frosinone of the Geological Map of Italy at l:100,000, 2nd edn. Servizio Geologico d' Italia, Rome

Acocella V, Funiciello R (2002) Transverse structures and volcanic activity along the Tyrrhenian margin of central Italy. Boll della Soc Geol Ital 121(1):739–747

Acocella V, Funiciello R (2006) Transverse systems along the extensional Tyrrhenian margin of central Italy and their influence on volcanism. Tectonics 25(2):TC2003

Acocella V, Faccenna C, Funiciello R (1996) Elementi strutturali della media Valle Latina. Boll Soc Geol Ital 115:501–518

Alberti A, Bergomi C, Catenacci V, Centamore E, Cestar G, Chiocchini M, Chiocchini U, Manganelli V, Molinari-Paganelli V, Panserl-Crescenzi C, Salvati L, Tilia Zuccari A (1975) Note illustrative del Foglio 389 Anagni. Carta Geologica d'Italia 1:50.000. Servizio Geologico d'Italia, Rome

Angelucci A, Brotzu P, Civitelli G, Morbidelli L, Traversa G (1974) Il vulcanismo pleistocenico della media Valle Latina (Lazio). Caratteristiche petrografiche e geologiche dei principali affioramenti lavici. Geol Romana 13:83–123

Ascenzi A, Mallegni F, Manzi G, Segre AG, Segre Naldini E (2000) A re-appraisal of Ceprano calvaria affinities with Homo erectus, after the new reconstruction.J. Hum Evol 39:443–450

Ascione A, Capalbo A, Capolongo D, Mazzoli S, Pazzaglia F, Valente E, Zattin M (2012) Uplift vs. denudation in the southern Apennines: geomorphologic evidence and constraints from terrestrial cosmogenic nuclides and apatite (U-Th)/He data. Rend Online Soc Geol Ital 21:1102–1104

Barberi F, Buonasorte G, Cioni R, Fiordelisi A, Foresi L, Iaccarino S, Laurenzi MA, Sbrana A, Vernia L, Villa IM (1994) Plio-Pleistocene geological evolution of the geothermal area of Tuscany and Latium. Mem Descr Carta Geol Ital 49:77–134

Basilone P, Civetta L (1975) Datazione K/Ar dell'attivita' vulcanica dei Monti Ernici (Latina). Rend della Soc Ital di Mineral e Petrol 31:175–179

Beaudoin A, Augier R, Jolivet L, Jourdon A, Raimbourg H, Scaillet S, Cardello GL (2017) Deformation behavior of continental crust during subduction and exhumation: strain distribution over the Tenda massif (Alpine Corsica, France). Tectonophysics 705:12–32

Bernoulli D (2001) Mesozoic-Tertiary carbonate platforms, slopes and basins of the external Apennines and Sicily. In: Vai GB, Martini P (eds) Anatomy of an Orogen: The Apennines and Adjacent Mediterranean Basins. Kluwer Academic Publishers, Dordrecht, pp 307–325

Blumetti AM, Guerrieri L (2007) Fault-generated mountain fronts and the identification of fault segments: implications for seismic hazard assessment. Boll della Soc Geol Ital 126(2):307

Boari E, Conticelli S (2007) Mineralogy and petrology of associated Mg-RICH ultrapotassic, shoshonitic, and calc-alkaline rocks: The Middle Latin Valley monogenetic volcanos, Roman Magmatic Province, southern Italy. Canad Mineral 45(6):1443–1469

Boari E, Tommasini S, Laurenzi MA, Conticelli S (2009) Transition from ultrapotassic Kamafugitic to Sub-alkaline Magmas: Sr, Nd, and Pb isotope, trace element and 40Ar-39Ar age data from the middle Latin Valley Volcanic Field, Roman Magmatic Province, Central Italy. J Petrol 7:1327–1357

Bonechi B, Perinelli C, Gaeta M, Tecchiato V, Granati SF (2017) Experimental constraints on amphibole stability in primitive alkaline and calc-alkaline magmas. Period Mineral 86:231–245. https://doi.org/10.2451/2017PM735

Bonechi B, Perinelli C, Gaeta M (2020) Clinopyroxene growth rates at high pressure: constraints on magma recharge of the deep reservoir of the Campi Flegrei Volcanic District (south Italy). Bull Volcanol 82:5

Branco W (1877) I vulcani degli Ernici nella Valle del Sacco. Mem R Ace Lincei Ser 3(1):17 (**fig., Roma**)

Butler RW, Tavarnelli E, Grasso M (2006) Structural inheritance in mountain belts: an Alpine-Apennine perspective. J Struct Geol 28(11):1893–1908

Calamita F, Pizzi A (1994) Recent and active extensional tectonics in the southern Umbro-Marchean Apennines (central Italy). Mem Soc Geol It 48:541–548

Cardello GL, Doglioni C (2015) From Mesozoic rifting to Apennine orogeny: The Gran Sasso range (Italy). Gondwana Res 27:1307–1334

Cardello GL, Consorti L, Palladino DM, Carminati E, Carlini M, Doglioni C (2020) Tectonically controlled carbonate-seated maar-diatreme volcanoes: the case of the Volsci Volcanic Field, central Italy. J Geodyn 139:101763

Carminati E, Fabbi S, Santantonio M (2014) Slab bending, syn-subduction normal faulting, and out-of-sequence thrusting in the Central Apennines. Tectonics 33(4):530–551

Castellarin A, Colacicchi R, Praturion A (1978) Fasi distensive, trascorrenze e sovrascorrimenti lungo la linea Ancona-Anzio dal Lias al Pliocene. [Extensional, strike-slip, and compressional stages along the Ancona-Anzio lineament from Lias to Pliocene]. Geol Rom 17:161–189

Cavinato GP, Cosentino D, De Rita D, Funiciello R, Parotto M (1994) Tectonic-sedimentary evolution of intrapenninic basins and correlation with the volcano-tectonic activity in Central Italy. Mem Descr della Carta Geol Ital 49:63–76

Centamore E, Di Manna P, Rossi D (2007) Kinematic evolution of the Volsci Range: a new overview. Ital J Geosci 126:159–172

Centamore E, Dramis F, Di Manna P, Fumanti F, Milli S, Rossi D, Palombo MR, Palladino DM, Trigila R, Zanon V, Chiocchini M, Didaskalou P, Potetti M, Nisio S (2010) Note illustrative del Foglio 402 Ceccano. Carta Geologica d'Italia 1:50.000. Servizio Geologico d'Italia, Rome

Chiarabba C, Palano M (2017) Progressive migration of slab breakoff along the southern Tyrrhenian plate boundary: constraints for the present day kinematics. J Geodyn 105:51–61

Chiarabba C, Giacomuzzi G, Bianchi I, Agostinetti NP, Park J (2014) From underplating to delamination-retreat in the northern Apennines. Earth Planet Sci Lett 403:108–116

Cipollari P, Cosentino D (1991) La linea Olevano-Antrodoco: contributo della biostratigrafia alla sua caratterizzazione cinematica. Studi geologici camerti, n. speciale, pp 143–149

Civetta L, Innocenti F, Lirer L, Manetti P, Munno R, Peccerillo A, Poli G, Serri G (1979) Serie potassica ed alta in potassio dei Monti Ernici (Lazio Meridionale): considerazioni petrologiche e geochimiche. Rend della Soc Ital di Mineral Petrol 35:227–249.

Civetta L, Innocenti F, Manetti P, Peccerillo A, Poli G (1981) Geochemical characteristics of potassic volcanics from Mts. Ernici (southern Latium, Italy). Contrib Mineral Petrol 78(1):37–47

Conte AM, Dolfi D, Gaeta M, Misiti V, Mollo S (2009) Experimental constraints on evolution of leucite-basanite magma at 1 and 10–4 GPa : implications for parental compositions of Roman high-potassium magmas. Eur J Mineral 21:763–782. https://doi.org/10.1127/0935-1221/2009/0021-1934

Conticelli S, Marchionni S, Rosa D, Giordano G, Boari E, Avanzinelli R (2009) Shoshonite and sub-alkaline magmas from an ultrapotassic volcano: Sr–Nd–Pb isotope data on the Roccamonfina volcanic rocks, Roman Magmatic Province. Southern Italy. Contrib Mineral Petrol 157(1):41–63

Cosentino D, Cipollari P, Di Donato V, Sgrosso I (2002) The Volsci Range in the kinematic evolution of thenorthern and southern Apennine orogenetic system, Italian. J Geosci 1:209–218

Cosentino D, Asti R, Nocentini M, Gliozzi E, Kotsakis T, Mattei M, Esu D, Spadi M, Tallini M, Cifelli F, Pennacchioni M, Cavuoto G, Di Fiore V (2017) New insights into the onset and evolution of the central Apennine extensional intermontane basins based on the tectonically active L'Aquila Basin (central Italy). Geol Soc Am Bull 129(9–10):1314–1336

De Luca G (2011) La Rete Sismica regionale d'Abruzzo e sua integrazione con la RSN. In: Miscellanea INGV, Riassunti estesi del I° Workshop Tecnico Monitoraggio sismico del territorio nazionale: stato dell'arte e sviluppo delle reti di monitoraggio sismico, Roma 20–21 Decembre 2010, pp 22–23

Deino AL, Orsi G, de Vita S, Piochi M (2004) The age of the Neapolitan Yellow Tuff caldera-forming eruption (Campi Flegrei caldera, Italy) assessed by 40Ar/39Ar dating method. J Volcanol Geotherm Res 133:157–170. https://doi.org/10.1016/S0377-0273(03)00396-2

Devoto G (1967) Le brecce calcaree mioceniche nell'alta Valle Roveto tra Castellafiume e Canistro (Frosinone, Lazio meridionale). Geol Romana 6:75–86

Di Luzio E, Arienzo I, Boccuti S, De Meo A, Sottili G (2018) Chemical-petrographic and isotopic analyses of the volcanic stone pavement along the ancient Appia route at the Aurunci mountains pass (central Italy): insights for possible provenance. Geoarcheology 34:5

Doglioni C, Mongelli F, Pieri P (1994) The Puglia uplift (SE Italy): an anomaly in the foreland of the Apenninic subduction due to buckling of a thick continental lithosphere. Tectonics 13(5):1309–1321

Elizabeth M. Niespolo, Daniel Rutte, Alan L. Deino, Paul R. Renne, (2017) Intercalibration and age of the Alder Creek sanidine $^{40}Ar/^{39}Ar$ standard. Quat Geochronol 39:205–213

Fabbi S, Santantonio M (2018) First report of a Messinian coralgal facies in a terrigenous setting of Central Apennines (Italy) and its palaeogeographic significance. Geol J. https://doi.org/10.1002/gj.3267

Faccenna C, Davy P, Brun JP, Funiciello R, Giardini D, Mattei M, Nalpas T (1996) The dynamics of back-arc extension: an experimental approach to the opening ofthe Tyrrhenian Sea. Geophys J Int 126:781–795

Fornaseri M (1985) Geochronology of volcanic rocks from Latium (Italy). Rend della Soc Ital Mineral Petrol 40(1):73–106

Freda C, Gaeta M, Palladino DM, Trigila R (1997) The Villa Senni Eruption (Alban Hills, central Italy): the role of H2O and CO2 on the magma chamber evolution and on the eruptive scenario. J Volcanol Geotherm Res 78(1–2):103–120

Freda C, Gaeta M, Karner DB, Marra F, Renne PR, Taddeucci J, Scarlato P, Christensen JN, Luigi Dallai L (2006) Eruptive history and petrologic evolution of the Albano multiple maar (Alban Hills, Central Italy). Bulletin of Volcanology 68(6):567–591

Freda C, Gaeta M, Misiti V, Mollo S, Dolfi D, Scarlato P (2008) Magma–carbonate interaction: An experimental study on ultrapotassic rocks from Alban Hills (Central Italy). Lithos 101(3–4):397–415

Freda C, Gaeta M, Giaccio B, Marra F, Palladino DM, Scarlato P, Sottili G (2011) CO2-driven large mafic explosive eruptions: the Pozzolane Rosse case study from the Colli Albani Volcanic District (Italy). Bulletin of Volcanology 73(3):241–256

Frepoli A, Marra F, Maggi C, Marchetti A, Nardi A, Pagliuca NM, Pirro M (2010) Seismicity, seismogenic structures and crustal stress field in the greater area of Rome (Central Italy). JGR. https://doi.org/10.1029/2009JB006322

Frepoli A, Cimini GB, De Gori P, De Luca G, Marchetti A, Monna S, Montuori C, Pagliuca NM (2017) Seismic sequences and swarms in the Latium–Abruzzo–Molise Apennines (Central Italy): new observations and analysis from a dense monitoring of the recent activity. Tectonophysics 712–713:312–329. https://doi.org/10.1016/j.tecto.2017.05.026

Frezzotti ML, De Astis G, Dallai L, Ghezzo C (2007) Coexisting calc-alkaline and ultrapotassic magmatism at Monti Ernici, Mid Latina Valley (Latium, central Italy). Eur J Mineral 19(4):479–497

Gaeta M, Fabrizio G, Cavarretta G (2000) F-phlogopites in the Alban Hills Volcanic District (Central Italy): indications regarding the role of volatiles in magmatic crystallisation. J Volcanol Geotherm Res 99(1–4):179–193

Gaeta M, Freda C, Christensen JN, Dallai L, Marra F, Karner DB, Scarlato P (2006) Evolution of the Mantle Source for Ultrapotassic Magmas of the Alban Hills Volcanic District (Central Italy). Lithos 86:330–346. https://doi.org/10.1016/j.lithos.2005.05.010

Gaeta M, Freda C, Marra F, Arienzo I, Gozzi F, Jicha B, Di Rocco T (2016) Paleozoic metasomatism at the origin of Mediterranean ultrapotassic magmas: constraints from time-dependent geochemistry of Colli Albani volcanic products (Central Italy). Lithos 244:151–164

Ghisetti F, Vezzani L (1999) Depth and modes of Pliocene-Pleistocene crustal extension of the Apennines (Italy). Terra Nova 11(2–3):67

Giaccio B, Leicher N, Mannella G, Monaco L, Regattieri E, Wagner B, Zanchetta G, Gaeta M, Marra F, Nomade S, Palladino DM, Pereira A, Scheidt S, Sottili G, Wonik T, Wulf S, Zeeden C, Ariztegui D, Cavinato GP, Dean J, Florindo F, Leng M, Macrì P, Niespolo E, Renne PR, Rolf C, Sadori L, Thomas C, Tzedakis C (2019) Extending the tephra and palaeoenvironmental record of the Central Mediterranean back to 430 ka: a new core from Fucino Basin, central Italy. Quat Sci Rev 225:106003

Giacomuzzi G, Civalleri M, De Gori P, Chiarabba C (2012) A 3D Vs model of the upper mantle beneath Italy: Insight on the geodynamics of central Mediterranean. Earth Planet Sci Lett 335:105–120

Gozzi F, Gaeta M, Freda C, Mollo SD, Rocco T, Marra F, Dallai L, Pack A (2013) Primary magmatic calcite reveals origin from crustal carbonate. Lithos 190–191:191–203

Gupta AK (1972) The system forsterite-diopside-akermanite-leucite and its significance in the origin of potassium-rich mafic and ultramafic rocks. Am Mineral 57:1242–1259

Hippolyte JC, Angelier J, Roure F (1994) A major geodynamic change revealed by Quaternary stress patterns in the southern Apennines (Italy). Tectonophysics 230(3–4):199–210

Jicha BR, Singer BS, Sobol P (2016) Re-evaluation of the ages of 40Ar/39Ar sanidine standards and supereruptions in the western U.S. using a Noblesse multi-collector mass spectrometer. Chem Geol 431:54–66

Karner DB, Renne PR (1998) 40Ar/39Ar geochronology of Roman Volcanic Province tephra in the Tiber River Valley: age calibration of middle Pleistocene sea-level changes. Geol Soc Am Bull 110:740–747

Koopman A (1983) Detachment tectonics in the central Apennines, Italy. Geol Ultraiectina 30(1983):1–55

Koornneef JM, Nikogosian I, van Bergen MJ, Vroon PZ, Davies GR (2019) Ancient recycled lower crust in the mantle source of recent Italian magmatism. Nat Commun 10(1):1–10

Kuiper KF, Deino A, Hilgen FJ, Krijgsman W, Renne PR, Wijbrans JR (2008) Synchronizing Rock Clocks of Earth History. Science 320(5875):500–504

Lavecchia G (1985) Il sovrascorrimento dei Monti Sibillini: analisi cinematica e strutturale. Boll della Soc Geol Ital 104:161–194

Lavecchia G, Brozzetti F, Barchi M, Menichetti M, Keller JV (1994) Seismotectonic zoning in east-central Italy deduced from an analysis of the Neogene to present deformations and related stress fields. GSA Bull 106(9):1107–1120

Lucente P, Speranza F (2001) Belt bending driven by lateral bending of subducting lithospheric slab: Geophysical evidences from the Northern Apennines (Italy). Tectonophysics 337(1):53–64. https://doi.org/10.1016/S0040-1951(00)00286-9

Malinverno A, Ryan WBF (1986) Extension in the Tyrrhenian sea and shortening in the Apennines as results of arc migration driven by sinking of the lithosphere. Tectonics 5:227–245

Manzi G (2015) Humans of the Middle Pleistocene: the controversial calvarium from Ceprano (Italy) and its significance for the origin and variability of Homo heidelbergensis. Quat Int 411:254–261. https://doi.org/10.1016/j.quaint.2015.12.047

Mariucci MT, Montone P (2019) IPSI 1.3, Database of Italian present-day stress indicators, Istituto Nazionale di Geofisica e Vulcanologia (INGV). https://doi.org/10.6092/INGV.IT-IPSI.1.3DATABASE

Marra F, Florindo F (2014) The subsurface geology of Rome: sedimentary processes, sea-level changes and astronomical forcing. Earth Sci Rev 136:1–20. https://doi.org/10.1016/j.earscirev.2014.05.001

Marra F, Freda C, Scarlato P, Taddeucci J, Karner DB, Renne PR, Gaeta M, Palladino DM, Trigila R, Cavarretta G (2003) Post-caldera activity in the Alban Hills Volcanic District (Italy): 40Ar/39Ar geochronology and insights into magma evolution. Bull Volc 65:227–247

Marra F, Taddeucci J, Freda C, Marzocchi W, Scarlato P (2004) Recurrence of volcanic activity along the Roman Comagmatic Province (Tyrrhenian margin of Italy) and its tectonic significance. Tectonics 23:TC4013. https://doi.org/10.1029/2003TC001600

Marra F, Karner DB, Freda C, Gaeta M, Renne PR (2009) Large mafic eruptions at the Alban Hills Volcanic District (Central Italy): chronostratigraphy, petrography and eruptive behavior. J Volc Geoth Res 179:217–232. https://doi.org/10.1016/j.jvolgeores.2008.11.009

Marra F, Sottili G, Gaeta M, Giaccio B, Jicha B, Masotta M, Palladino DM, Deocampo D (2014) Major explosive activity in the Sabatini Volcanic District (central Italy) over the 800–390 ka interval: geochronological—geochemical overview and

tephrostratigraphic implications. Quat Sci Rev 94:74–101. https://doi.org/10.1016/j.quascirev.2014.04.010

Marra F, Gaeta M, Giaccio B, Jicha B, Palladino D, Polcari M, Sottili G, Taddeucci J, Florindo F, Stramondo S (2016) Assessing the volcanic hazard for Rome: 40Ar/39Ar and In-SAR constraints on the most recent eruptive activity and present-day uplift at Colli Albani Volcanic District. GRL 43:6898–6906. https://doi.org/10.1002/2016GL069518

Marra F, Florindo F, Jicha BR, Nomade S, Palladino DM, Pereira A, Sottili G, Tolomei C (2019) Volcano-tectonic deformation in the Monti Sabatini Volcanic District at the gates of Rome (central Italy): evidence from new geochronologic constraints on the Tiber River MIS 5 terraces. Sci Rep 9:11496. https://doi.org/10.1038/s41598-019-47585-8

Marra F, Jicha BR, Palladino DM, Gaeta M, Costantini L, Di Buduo GM (2020a) 40Ar/39Ar single crystal dates from pyroclastic deposits provide a detailed record of the 590–240 ka eruptive period at the Vulsini Volcanic District (central Italy). J Volcanol Geotherm Res 398:106904

Marra F, Castellano C, Cucci L, Florindo F, Gaeta M, Jicha B, Palladino DM, Sottili G, Tertulliani A, Tolomei C (2020b) Monti Sabatini and Colli Albani: the dormant twin volcanoes at the gates of Rome. Sci Rep 10:8666. https://doi.org/10.1038/s41598-020-65394-2

Molli G (2008) Northern Apennine-Corsica orogenic system: an updated overview. Geol Soc Lond 298(1):413–442

Montone P, Mariucci MT (2016) The new release of the Italian contemporary stress map. Geophys J Int 205(3):1525–1531. https://doi.org/10.1093/gji/ggw100

Morewood NC, Roberts GP (2000) The geometry, kinematics and rates of deformation within an en échelon normal fault segment boundary, central Italy. J Struct Geol 22(8):1027–1047

Murchison RI (1850) On the Earlier Volcanic Rocks of the Papal States, and the adjacent parts of Italy. Quart J Geol Soc 6(1–2):281–310

Narcisi B (1986) Ricerche di tefracronologia nella media e bassa Valle Latina. Mem Soc Geol It 35:909–912

Niespolo EM, Rutte D, Deino AL, Renne PR (2017) Intercalibration and age of the Alder Creek sanidine $^{40}Ar/^{39}Ar$ standard. Quaternary Geochronology 39:205–213

Nikogosian IK, van Bergen MJ (2010) Heterogeneous mantle sources of potassium-rich magmas in central-southern Italy: Melt inclusion evidence from Roccamonfina and Ernici (Mid Latina Valley). J Volcanol Geotherm Res 197(1–4):279–302

Nomade S, Muttoni G, Guillou H, Robin E, Scardia G (2011) First 40Ar/39Ar age of the Ceprano man (central Italy). Quat Geochronol 6:453–457

Palladino DM, Gaeta M, Marra F (2001) A large K-foiditic hydromagmatic eruption from the early activity of the Alban Hill Volcanic District, Italy. Bull Volcanol 63:345–359

Palladino DM, Simei S, Sottili G, Trigila R, Groppelli G (2010) Integrated approach for the reconstruction of stratigraphy and geology of Quaternary volcanic terrains: an application to the Vulsini Volcanoes (central Italy). Stratigr Geol Volc Areas Geol Soc Am 464:63–84

Parotto M (1971) Stratigraphy and tectonics of the Eastern Simbruini and Western Marsica Ranges (Central Apennines-Italy). Atti Acc. Naz. Lincei, Mem., s. 8, Roma 10(4):91–170

Parotto M, Praturlon A (1975) Geological summary of the Central Appenines. In: Ogniben L, Parotto M, Praturlon A (eds) Structural model of Italy. Quad. Ric. Scient., CNR-Rome, 90:257–311

Parotto M, Tallini M (2013) Geometry and kinematics of the Montelanico-Carpineto Backthrust (Lepini Mts., Latium) in the hanging-wall of the early Messinian thrust front of the central Apennines: implications for the Apennine chain building, Italian. J Geosci 132:274–289

Pasquarè G, Serri G, Vezzoli L (1985) Carta geologica dell'area della MediaValle Latina. Scala 1:50 000. Progetto finalizzato geodinamica. Sottoprogetto: sorveglianza dei vulcani e rischio vulcanico. In: Carte tematiche sul vulcanismo recente.Istituto di Geologia, University of Milan, Milan

Patacca E, Scandone P (1989) Post-Tortonian mountain building in the Apennines: the role of the passive sinking of a relic litho-spheric slab. In: Boriani A, Bonafede M, Piccardo GB, Vai GB (eds) The Lithosphere in Italy: advance in earth science research. C.N.R., Acc. Nazionale dei Lincei, Rome, pp 157–176

Peccerillo A (2017) Cenozoic Volcanism in the Tyrrhenian Sea Region. IAVCEI, Advances in Volcanology, Springer (ed.), Barcelona, Spain, p 399

Pereira A, Nomade S, Moncel MH, Voinchet P, Bahain JJ, Biddittu I, Falguères C, Giaccio B, Manzi G, Parenti F, Scardia G, Scao V, Sottili G, Vietti A (2018) Integrated geochronology of Acheulian sites from the southern Latium (Central Italy): Insights on human-environment interaction and the technological innovations during the MIS 11-MIS 10 period. Quat Sci Rev 187:112–129

Perinelli C, Gaeta M, Bonechi B, Granati SF, Freda C, D'Antonio M, Stagno V, Sicola S, Romano C (2019) Effect of water on the phase relations of primitive K-basalts: implications for high-pressure differentiation in the Phlegraean Volcanic District magmatic system. Lithos 342–343:530–541

Perini G, Francalanci L, Davidson JP, Conticelli S (2004) Evolution and genesis of magmas from Vico Volcano, Central Italy: multiple differentiation pathways and variable parental magmas. J Petrol 45(1):139–182

Piccardi L, Gaudemer Y, Tapponnier P, Boccaletti M (1999) Active oblique extension in the central Apennines (Italy): evidence from the Fucino region. Geophys J Int 139(2):499–530

Pierantoni PP, Penza G, Macchiavelli C, Schettino A, Turco E (2020) Kinematics of the Tyrrhenian–Apennine system and implications for the origin of the Campanian magmatism. Vesuvius, Campi Flegrei, and Campanian Volcanism. Elsevier, Amsterdam, pp 33–56

Pizzi A, Galadini F (2009) Pre-existing cross-structures and active fault segmentation in the northern-central Apennines (Italy). Tectonophysics 476(1–2):304–319

Ponzi G (1858a) Sui rinvenimenti dei vulcani spenti degli Ernici nella Valle Latina. Atti Pont. Accad. Nuovi Linc., vol 11. Rome

Ponzi G (1858b) Osservazioni geologiche sulle provincie di Frosinone e di Velletri. Atti Pont N Lincei 11:170–172 (**Roma**)

Pouchou JL, Pichoir F (1991) Quantitative analysis of homogeneous or stratified microvolumes applying the model "PAP". Electron probe quantitation. Springer, Boston, MA, pp 31–75

Radicati di Brozolo F, Di Girolamo P, Turi B, Oddone M (1988) ^{40}Ar-^{39}Ar and K-Ar dating of K-rich rocks from the Roccamonfina Volcano, Roman Comagmatic Region, Italy. Geochim Cosmochim Acta 52(6):1435–1441

Rosenbaum G, Piana Agostinetti N (2015) Crustal and upper mantle responses to lithospheric segmentation in the northern Apennines. Tectonics 34(4):648–661

Rosenbaum G, Gasparon M, Lucente FP, Peccerillo A, Miller MS (2008) Kinematics of slab tear faults during subduction segmentation and implications for Italian magmatism. Tectonics 27:TC2008

Rouchon V, Gillot PY, Quidelleur X, Chiesa S, Floris B (2008) Temporal evolution of the Roccamonfina volcanic complex (Pleistocene), Central Italy. J Volcanol Geoth Res 177(2):500–514

Sani F, Del Ventisette C, Montanari D, Coli M, Nafissi P, Piazzini A (2004) Tectonic evolution of the internal sector of the Central Apennines, Italy. Mar Petrol Geol 21(10):1235–1254

Sartori R, Torelli L, Zitellini N, Carrara G, Magaldi M, Mussoni P (2004) Crustal features along a W-E Tyrrhenian transect from

Sardinia to Campania margins (Central Mediterranean). Tectonophysics 383(3–4):171–192

Sottili G, Palladino DM, Marra F, Jicha B, Karner DB, Renne P (2010) Geochronology of the most recent activity in the Sabatini Volcanic District, Roman Province, central Italy. J Volc Geoth Res 196:20–30. https://doi.org/10.1016/j.jvolgeores.2010.07.003

Sottili G, Arienzo I, Castorina F, Gaeta M, Giaccio B, Marra F, Palladino DM (2019) Time-dependent Sr and Nd isotope variations during the evolution of the ultrapotassic Sabatini Volcanic District (Roman Province, central Italy). Bull Volc. https://doi.org/10.1007/s00445-019-1324-7

Spakman W (1991) Delay-time tomography of the upper mantle below Europe, the Mediterranean, and Asia Minor. Geophys J Int 107:309–332

Spakman W, Van Der Lee S, Van Der Hilst R (1993) Travel-time tomography of the European±Mediterranean mantle down to 1400 km. Phys Earth Planet Int 79:3–74

Rocco TD, Freda C, Gaeta M, Mollo S, Dallai L (2012) Magma Chambers Emplaced in Carbonate Substrate: Petrogenesis of Skarn and Cumulate Rocks and Implications for CO2 Degassing in Volcanic Areas. J Petrol 53(11):2307–2332

Valentine GA, Perry FV (2007) Tectonically controlled, time-predictable basaltic volcanism from a lithospheric mantle source (central Basin and Range Province, USA). Earth Planet Sci Lett 261:201–216

Valentine GA, Sottili G, Palladino DM, Taddeucci J (2015) Tephra ring interpretation in light of evolving maar-diatreme concepts: Stracciacappa maar (central Italy). J Volcanol Geotherm Res 308:19–29. https://doi.org/10.1016/j.jvolgeores.2015.10.010

Villa IM, Buettner A (2009) Chronostratigraphy of Monte Vulture volcano (southern Italy): secondary mineral microtextures and 39Ar-40Ar systematics. Bull Volc 71(10):1195–1208